MULTI-DIMENSIONAL CHATTER STABILITY OF PARALLEL (SIMULTANEOUS) TURNING OPERATIONS

by

MILAD AZVAR

Submitted to the Graduate School of Engineering and Natural Sciences

in partial fulfillment of the requirements for the degree of

Master of Science

Sabancı University

June 2017

MULTI-DIMENSIONAL CHATTER STABILITY OF PARALLEL (SIMULTANEOUS) TURNING OPERATIONS

Approved by:

Prof. Dr. Erhan Budak (Thesis Advisor)

Prof. Dr. Ali Kosar

Assoc. Prof. Dr. Ender Cigeroglu

Date of approval June 30th, 2017

To the memory of my mother for her never-ending love and sacrifices;

and to my father who is the best part of everyday.

MULTI-DIMENSIONAL CHATTER STABILITY OF PARALLEL (SIMULTANEOUS) TURNING OPERATIONS

Milad Azvar

Manufacturing Engineering, MSc. Thesis, 2017

Thesis Supervisor: Prof Dr. Erhan Budak

ABSTARCT

Simultaneous turning with extra cutting edges increases the material removal rate (MRR), and thus the productivity of the process. On one hand, chatter instability could be a fatal threat to the productivity and part quality in simultaneous turning operations of slender and flexible workpieces. On the other hand, stability of flexible part turning can be increased significantly if the process parameters are selected properly. In practice, however, ensuring a stable parallel turning of a flexible workpiece is approached by the costly process of trial and error. In order to tackle this problem, a multi-dimensional model for chatter stability analysis of parallel turning operation is presented where the effects of components' dynamics, i.e. workpiece and cutters, in addition to insert's geometry are accounted for. The stability model is formulated for two configurations of the parallel turning operation in frequency and time domains, and verified experimentally. Chatter-free and high productivity cutting conditions are determined through optimal parameter selection employing stability maps generated for each configuration.

Keywords: Simultaneous turning, Multi-directional chatter, Flexible components, Insert geometry

PARALEL TORNALAMA (EŞ ZAMANLI) OPERASYONUN ÇOK BOYUTLU TIRLAMA KARARLILIĞI

Milad Azvar

Üretim Mühendisliği, Yüksek Lisans Tezi, 2017

Tez Danışmanı: Prof. Dr. Erhan Budak

ÖZET

Ekstra kesim kenarları ile eş zamanlı tornalama Talaş kaldırma oranı arttırır ve böylece sürecin verimliliği artar. Bir yandan, silindir ve esnek iş parçalarında tırlama kararsızlığı, eşzamanlı tornalama süreci verimliliğine ve parça kalitesine bir tehdit oluşturabilir. Bunun yanısıra, süreç değişkenleri uygun bir şekilde seçilirse esnek parçaların tornalama kararlılığı önemli ölçüde artabilir. Ancak uygulamada, esnek iş parçasının kararlı paralel tornalanmasından emin olmak maliyetli bir deneme yanılma süreciyle gerçekleştirilir. Bu sorunun üstesinden gelmek amacıyla paralel tornalama için çok boyutlu bir tırlama kararlılığı analiz modeli sunulmuştur. Bileşen dinamikleri, örneğin iş parçası ve kesiciler ayrıca kesici uç geometrisi hesaba katılmıştır. Kararlılık modeli zaman ve frekans domenlerᵢnde paralel tornalama operasyonu için formule edilmiştir ve deneysel olarak doğrulanmıştır. Tırlamasız ve yüksek verimli kesme şartları her iki biçim için oluşturulan kararlılık haritasını kullanılarak seçilen en iyi değişkenler ile belirlenir.

Anahtar kelimeler: Eş zamanlı tornalama, Çok yonlu tırlama, Esnek bileşenler, Kesici uç geometrisi

ACKNOWLEDGMENT

First and foremost, I would like to extend my deepest appreciation to my supervisor, Professor Dr. Erhan Budak, who has always encouraged me to go beyond my limits. His excellence supervision, guidance and criticism during my master study is highly appreciated. Prof. Budak has set an example I hope to match someday.

Member of examining committee, Dr. Ali Kosar and Dr. Ender Cigeroglu, are greatly appreciated due to the time and consideration they spend on the evaluating and reviewing the thesis. Their comments and suggestions improved the quality of the work.

The fruitful discussion with Dr. Emre Ozlu and Dr. Daniel Bachrathy (of the Budapest University of Technology and Economics) on the formulation of the problem is highly acknowledged. Special thanks to Mr. Veli Naksiler for his useful assistance and comments on using the Mori Seiki NTX2000 CNC machine during the experiments. Also, thanks to the Maxima members, Ertuğrul Sadıkoğlu, Süleyman Tutkun, Tayfun Kalender, Ahmet Ergen, Anıl Sonugür, Dilara Albayrak and Esma Baytok for their technical support throughout the experiments.

I convey my special acknowledgement to Faraz, Nasim, Amin, Ada, Yaser, Sahand and Milad Hassani for their boundless helps, friendship and encouragement during my stay in Sabanci, for which I am very grateful. Also, I would like to express my gratitude to my colleagues in MRL, Batuhan, Mehmet, Mert Gürtan, Mert Kocaefe, Mohammad Hassan, Esra, Hamid, Kaveh and Arash to make a very friendly environment in the MRL that made my Master study memorable and unforgettable.

Words are not able to express my sincere appreciation to my father Omar, sisters Mina and Medya for their endless support, love and kindness in my life, especially when I was away from them in Turkey.

Finally, I want to express my gratitude to all of my friends at Sabanci and those who have not been mentioned by name, but assisted me during my master study.

TABLE OF CONTENTS

LIST OF FIGURES

LIST OF TABLES

LIST OF SYMBOLS

C_1 : Side edge cutting angle of the first tool

C_2 : Side edge cutting angle of the second tool

b_1 : Depth of cut of the first tool

b_2 : Depth of cut of the second tool

r_1 : Nose radius of the first tool

r_2 : Nose radius of the second tool

i : Inclination angle

α : Rake angle

f_0 : Feed velocity

F_f : Feed force

F_r : Radial force

be : Elemental depth of cut

be_{stable} : Stability limit for an element

φ : Local side edge angle

n : Number of element in the second tool

m : Number of elements in the first tool

n_{nose} : Number of elements in nose area of second tool

m_{nose} : Number of elements in nose area of first tool

O : Axial offset between the cutters

y : Displacement in radial direction

x : Displacement in feed direction

t : Time

τ : Spindle rotation period

G_{xx} : Direct transfer function in the feed direction

G_{yy} : Direct transfer function in the radial direction

G_{xy} : Cross transfer function

ω_c : Chatter frequency

Ω : Spindle speed

K_f : Feed force coefficient

K_r : Radial force coefficient

K_{ef} : Feed edge force coefficient

K_{er} : Radial edge force coefficients

f_n : Natural frequency

Chapter 1 INTRODUCTION

Metal cutting techniques, parallel with other technologies involved in manufacturing, e.g. material sciences, automation control and computers, have continued to advance in the last decades. Despite the unprecedented escalation in novel manufacturing technologies, e.g. additive manufacturing and hybrid manufacturing, metal cutting techniques hold the center of interest of automation, aerospace and mould industry in manufacturing of near net shape parts. Broad applications, productivity, efficiency and above all, accuracy of machining technologies distinguish them as preferred manufacturing techniques compared with their counterparts.

Yet, from the commercial stand point, machining industries are challenged to manufacture accurate parts in a limited time to maximize the profit. Hence, to remain in the focus of interest of manufacturing industries, machining technologies are obliged to secure the accuracy and productivity of products.

Tool wear, cooling strategies, operating parameters (i.e. feed rate, spindle speed and depth of cuts), part measurements, various induced errors, components' vibration and chatter instability, to mention but a few, are various factors that may contribute to the accuracy and productivity of the metal cutting techniques. Among them, that the chatter instability is considered as a most catastrophic threat to the part quality and process productivity is of no question which occurs in wide range of machining processes (see Figure 1.1).
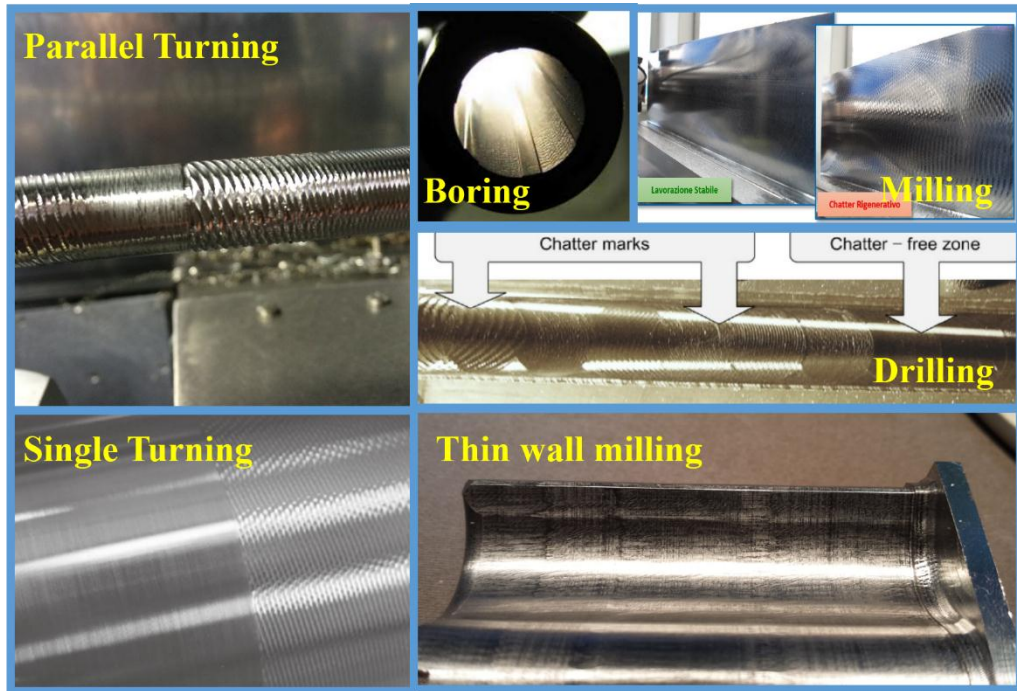
Figure 1.1. Chatter instability in different cutting process

Cutting process which undergone chatter phenomenon are susceptible to poor surface finish, tool breakage, tool wear, inordinate operating noise, and henceforth; reduced accuracy and productivity. In early years of twentieth century, to Fredrick Taylor, chatter was a strange phenomenon under which impede the operator to face the problem owing to unidentified nature of the process [1]. After preliminary observation of Taylor, almost half a century later, Tlusty and polacek [2] and Tobias and Fishwick [3], independently, identified regenerative chatter as the main source of chatter instability. In fact, Tlusty [4], identified mode coupling as another source for chatter stability where there is a vibration with identical natural frequency and phase in the plane of the motion, i.e. two directions. Nonetheless, it is well-known that regenerative chatter initiate instability earlier than mode coupling [4], and thus it has been in the center of researchers' interest.
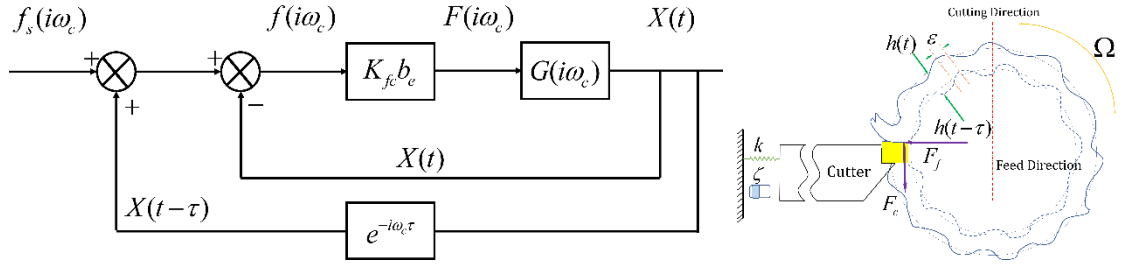
Figure 1.2. Regenerative chatter in an orthogonal turning operation

Oscillating tool leaves waves on workpiece's surface due to vibrations which influence the chip thickness. In the next revolution, by and large, if the width of cut is big enough, the oscillating wave's amplitude and its corresponding cutting force may increase. Successive increases in dynamic chip thickness and force called "regenerative chatter". Regenerative chatter can be simulated in a simple closed-loop block diagram as illustrated by Figure 1.2.

In Tlusty's and Polacek's [2] chatter stability theory, stable depth of cut can be determined for given dynamic properties of cutter and the workpiece in addition to cutting force coefficient for a simple but a practical orthogonal turning process. Merrit [6] provided similar results for orthogonal turning operation employing Nyquist stability criterion. However, applying previous models was not able to predict the chatter stability in milling operations due to time-dependent and intermittent nature of the process. An approximate model to predict chatter behavior in milling process was introduced by Tlusty [7] by considering average number of cutting flutes and also directional factor to reduce the problem to a time-invariant problem. Later on, Tlusty [8–10], developed a time domain model to simulate the chatter instability in milling operation. Minis [11-12], presented a novel formulation for dynamic modelling of a milling operation utilizing the Floquet's theorem and Fourier series expansion, and determine the stability limit based on Nyquist's stability criterion. Altintas and Budak [13], also presented an analytical model for predicating the chatter stability in milling process. In their model, time-varying behavior of the process is approximated with ZOA method in which only considers the constant coefficient in the Fourier series expansion of the directional factor to transform it to a time-independent problem. Even though, their method turned to be very time-efficient in constructing stability maps, the accurate results were only limited to high immersion conditions and/or high number of teeth. To improve the predictions, Budak [14-15]

3

developed a multi-frequency solution to the chatter stability modelling of the milling operation which consider higher number of harmonic frequency and consequently succeeded to predict the chatter instability in low immersion conditions.

Regardless of numerous investigation of chatter instability so far, chatter will remain as a crucial problem in the future of machining industry due to the several factors as listed below [5]:

- Demand for increase in Material Removal Rate (MRR)
- Limitation of machine tool manufacturer in designing well-damped structures[1]
- Inclination toward utilizing low friction guiding systems which are weakly damped
- Tendency to produce light-weight machine tools make them to be susceptible to unwanted vibration
- Flexible part machining

Nonetheless, since the identification of self-excited chatter instability, researchers and engineers had sought for procedures to suppress its unwanted vibration and therefore; eliminate the repercussion accompanied by the process. Some of these techniques are briefly mentioned in the next.

Stability Lobe Diagrams (SLD) are generated to avoid chatter instability by proper selection of process parameters, i.e. time delay (spindle speed since $\tau = 60/\Omega$) and depth of cut. Stability diagrams can be constructed for a machine tool structure with known dynamic properties, cutter geometry, force coefficient and process parameters. Figure 1.3 shows a common stability lobe diagram on a machine tool for a specific cutting process. As can be observed in Figure 1.3, system can be stable or unstable for each pair of spindle speed and depth of cut. Those combinations of the spindle speed and axial depth of cut lower than the limiting boundaries result in stable operation, whereas those points located in the upper parts leads to instable processes. Constructing such diagrams before initiating a cutting process help the machinist to select a proper spindle speed-depth of cut pair to

---

[1] FEM is able to predict natural frequencies and mode shapes of the machine tool components in early stages of designs. However, it may lead to false predictions when it comes to calculation of the damping properties of the structures. Such discrepancies mainly root in limitation of FEM in modelling of the joints as the main source of dissipating the energy [4].

avoid chatter. Obviously, seeking for a stable process by trial and error procedure would be a time and energy consuming process.
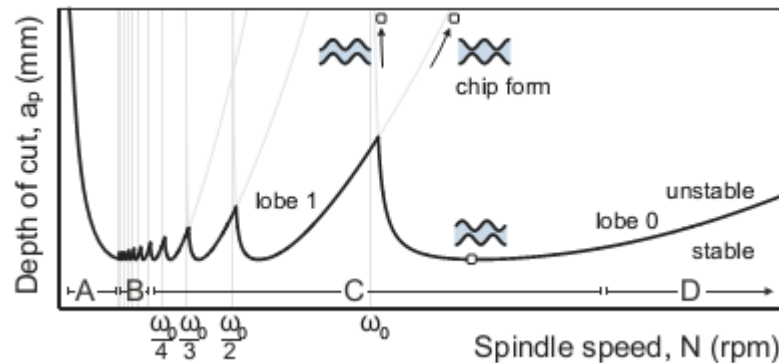
Figure 1.3. A common Stability Lobe Diagram (SLD) [5]

Spindle speed variation is an attenuating technique based on varying chatter wave modulation which are reasons behind instabilities [16]. In addition to spindle speed which can reduce regenerative chatter by varying the time delay in the process, variable pitch cutters can be utilized to intervene in time delay between chatter waves and improve stability [17-18]. Process damping, as well, can significantly hamper the disastrous effects of chatter instability in relatively low chatter frequencies and low spindle speeds [19-20]. Moreover, passive (TMDs[2] [21]) and active (Active tools [22], Active fixtures [23]) vibration absorber can effectively enhance the damping of the structure and result in stable processes. Recently, the idea of parallel machining has been conceived not only because of its favorable MRR, but also because of its ability to suppress chatter vibration during flexible part machining.

Since in this thesis the focus is on the parallel machining operations, general aspects of the such processes will be further elaborated in the next.

Parallel machining has received considerable attention in various manufacturing industries owing to their advantageous compared with traditional single operations. Clearly, employing extra cutting tools simultaneously will increase the material removal rate and obviously the productivity of the parallel processes. Furthermore, additional process and geometry parameters may be tuned for enhanced stability in simultaneous turning. For instance, utilizing two cutters with 180 degrees of difference in radial direction may results in cancelling the forces acting on the workpiece, and thus

---

[2] Tuned Mass Dampers

suppressing the chatter vibration. Moreover, radial angle between the cutters, for example, can be selected in a way to modify the dynamic chip thickness modulation for enhanced stability. Also, dynamics of the different components can be tuned to reduce the chatter vibration during the parallel machining. Similarly, extra process geometry while parallel turning, i.e. nose radius, inclination angle, rake angle and side edge cutting angle of the insert, can effectively be selected to observe the best stability behavior. And finally, different configuration of the components, i.e. cutters and workpiece, respect to each other, provide ability to perform various types of operation at the same time. Neither of aforementioned parameters can be modified in conventional turning which make the parallel turning pioneer to their traditional counterparts. Nevertheless, dynamics and chatter stability analysis of a simultaneous turning operation become further complicated because of the presence of various dynamic interactions between different components of the system in comparison with conventional turning operation. In case of a relatively rigid workpiece, the cutters may be coupled via the structure (turret and tool holder) or shared cutting surface. Intuitively, if neither of previous coupling scenarios exist, tools perform single mode turning operation with no coupling. It should be noted that during cutting a flexible workpiece, in addition to coupling through the shared surface or structure of the turret, components are coupled via the workpiece structure. Given above information, it is essential to have a comprehensive perspective over the dynamic and geometrical modelling of parallel turning operation in order to ensure a stable process by appropriate selection of process and geometry parameters.

1.1 Literature Survey

Chatter instability may results in jeopardizing enhanced productivity in parallel turning operations [24-25]. However, parallel machining can be employed as a chatter suppression technique in machining of flexible workpieces [5] and machining with flexible tools [25-26]. In parallel turning of a flexible workpiece, not only the tools' dynamics and their dynamic interaction but also the dynamics of the workpiece are crucial factors in stability analysis of the process. Consequently, ensuring a chatter-free cutting condition requires an appropriate selection of process parameters and process geometry which is achievable by having a precise and comprehensive insight into the modeling of the process geometry and dynamics. Even though, the number of publications on the one-dimensional chatter stability analysis is considerably high and go back to almost half a

century ago [2-3], there are few authors who investigated a general model for stability analysis of turning operations. Rao [27] developed an analysis in which the nose radii and cross-coupling effects between radial and axial displacement, in addition to sensitivity of the cutting force coefficients to smaller chip thicknesses has been taken into account. Later, Ozlu and Budak [28] presented an analytical multi-dimensional model to predict the stability limits in turning and boring processes. Their model considers all major parameters of the process geometry such as oblique angle, approach angle and nose radius, and more importantly the dynamic effects of tool and workpiece in different directions. Results in [28] shows that true geometry of the insert plays a vital role in the chatter stability of flexible part turning. In fact, by increasing the nose radii and side edge cutting angle of the insert absolute chatter stability of the process decrease drastically. Nonetheless, until recently, dynamics and stability of parallel turning operation has not been investigated extensively. Lazoglu [29] proposed a time-domain approach to stability of parallel turning system with two tools which are clamped on different turrets and cut different surfaces. The model includes the effect of both the tools' and the workpiece's dynamics. They demonstrated that for relatively flexible workpiece system, the stability limit in a conventional turning operation is slightly higher than the parallel process limit. Ozdoganlar and Enders [30] proposed a stability model for parallel turning operation of a symmetric system and verified their results through the experiments. Ozturk and Budak [25] proposed both frequency and time domain models for the stability of an orthogonal multi-delay parallel turning operation. In their model, the tools were coupled through the shared surface while each of the tools was cutting different depth of cuts. Results demonstrate that stability limit could increase according to the dynamic interaction between the tools creating an absorber effect. The results in [25] indicates MRR can be enhanced not only by exploiting extra cutting edges but also by proper selecting the process parameters. Brecher et al. [26] investigated the parallel turning operation in which cutters removed the same depth of cut from the workpiece considering various dynamic coupling of the tools through the machine structure. Frequency and time domain approaches supported that the radial angle between the tools has remarkable effects on shifting the stable depth of cut for the dynamically coupled tools [26]. In contrast, no significant dependence of the chatter stability limit to the radial angle were observed while using tools with independent dynamics transfer functions. Ozturk et al. [31] used two different cutting strategies in parallel turning, i.e. cutters cutting a shared surface of the rigid workpiece and cutters clamped on a turret removing material from different

7

surfaces of a rigid workpiece. Moreover, Ozturk et al. [31] for the first time emphasized the prominent influence of natural frequency ratio of the tools in chatter stability of parallel turning operations. They demonstrated that by adding or removing mass, and changing the tool holder's length, the system can be tuned for enhanced productivity. The results denoted that dynamically identical tools give the worst stability limit. Similarly, Reith at el.[32-33], theoretically and experimentally scrutinized the effect of tuning natural frequency of the tools and dynamic vibration absorbing potential on the stability of parallel turning operation. They have confirmed that using detuned cutters in parallel turning the MRR can be increased by shifting the stability boundaries upwards. Recently, Reith et al. [34] utilized non-proportional damping to model the multi-cutter system which includes the dynamic coupling between the cutters via the fixture. Their results showed that presence of non-proportional damping further improves the stable boundaries of a detuned cutter system. Although several works have been reported mainly focusing on 1D dynamic modeling of chatter stability for parallel turning operations and tuning the process to suppress chatter instability, multi-dimensional chatter stability considering true geometry of cutting tool and workpiece dynamics for different parallel turning strategies has not been investigated so far.

1.2. Objectives

The primary objective of this study is to develop a general multi-dimensional stability model for different parallel turning strategies. Two main strategies where tools can cut the workpiece's surface, i.e. cutting a shared surface, or cutting different surfaces are presented. For the first time in modeling of parallel turning, main parameters of process geometry, i.e. side edge cutting angle and nose radii of the tools, are included in the analysis. Moreover, tool and workpiece dynamic compliance effects are accounted for in the model to improve the stability limit predictions. Frequency and time domain stability models are developed for parallel turning strategies where effects of process parameters on the chatter behavior are thoroughly investigated. Simulation predictions are compared and verified with the experimental results. Finally, for each parallel turning strategy, best process parameters for a stability-guaranteed and productivity-enhanced operation is identified.

1.3. Organization of the Thesis

The thesis is outlined as follows:

- In chapter two, configurability in parallel turning process is emphasized as an advantageous of the process compared with their conventional counterparts. Two different strategies (of interest) in parallel turning operation has been introduced. Different dynamic coupling scenarios for each strategy is elaborated. Finally, practical limitation or advantageous of each strategy has been magnified.

- In chapter three, a multi-dimensional chatter stability model is presented for introduced strategies in chapter two. Workpiece and cutter's flexibility is accounted for in developing the formulations. Additionally, true geometry of the inserts is considered. After deriving the eigenvalue problem, a numerical MDBM is utilized to solve the equation in the frequency domain. To have a better insight into the chatter phenomena and its initiation, a time domain model is constructed in MATLAB/Simulink based on the chip thickness definition.

- In chapter four, simulated results of frequency and time domain model is compared with the experimental results. Stability maps for each parallel turning strategy and flexibility scenarios (four cases in total) is generated and good agreement is observed with test results. Effect of cutters' depth of cut in addition to inserts' geometry parameter's is investigated on the stability maps. Provided stability map in the current thesis give the operator a good insight over the parameter selection in parallel turning operation to gain a stable process where was performed as a trial and error procedure previously.

- In chapter five, the summary of the thesis is presented along with major conclusion of the thesis.

Chapter 2 **DIFFERENT STRATEGIES IN PARALLEL TURNING OPERATIONS**

Configurability is another advantage of parallel turning operations. Although increased process and geometry parameters in addition to dynamic interactions among the components may hamper controlling the chatter instability, adjusting proper cutting conditions in each configuration can be advantageous for attenuating the chatter vibrations. In the following, two main strategies used in this study is presented.

2.1. Cutters on Different Turrets Cutting a Shared Surface

Figure 2.1 demonstrates a schematic illustration of a parallel turning operation in which cutters mounted on different turrets machine a shared surface of the workpiece. As can be observed in Figure 2.1, dynamic contribution of different components, i.e. the cutters, the workpiece and the spindle structure, has been considered.
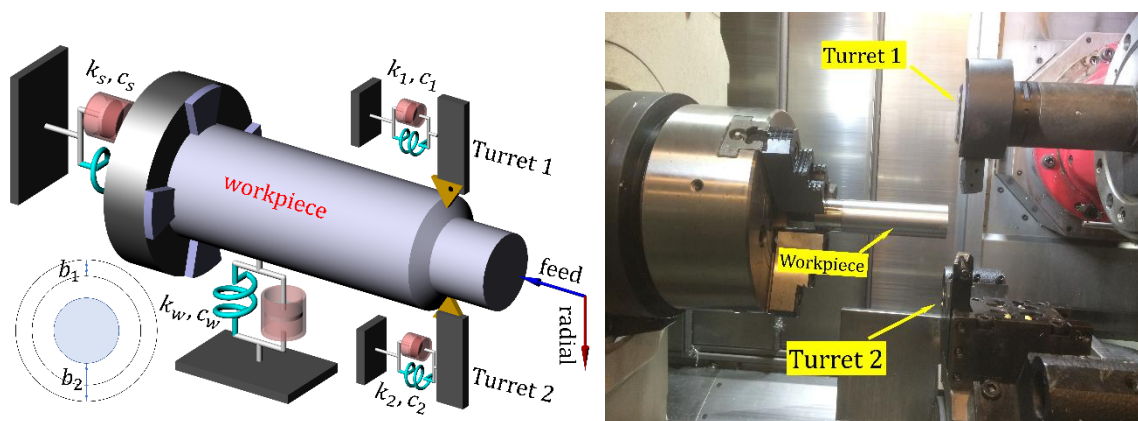
Figure 2.1. Cutters mounted on different turrets cutting a shared surface (coupled via the shared surface

Generally, given geometry of most of turning operations, tools are considered to be flexible in the feed direction while workpieces are considered to be flexible in the radial

direction. However, in current study, a general formulation is presented in which dynamic effect of the cutters in radial direction, in addition to dynamic effects of the workpiece in the feed direction can be easily taken into account. It is noteworthy that various components in the process can experience different coupling scenarios. During cutting a relatively rigid workpiece by flexible cutters, cutters do not have any dynamic coupling through the structures. In fact, dynamic forces acting on one of the cutters cannot influence the dynamic force of the another one. However, in this configuration, even though the tools are not dynamically coupled via the, waviness on the surface due to vibrations of one of the tools causes variation of the chip thickness on the other tool; hence, tools are dynamically dependent. While cutting the shared surface of a flexible workpiece, on the other hand, in addition to dynamic coupling of the cutters via the shared surface, the cutters are coupled via the workpiece as well. As a matter of fact, radial dynamic forces acting upon on one of the cutters can affect the radial dynamic force applied on the other one owing to dynamic cross transfer function created by radial flexibility of the workpiece.
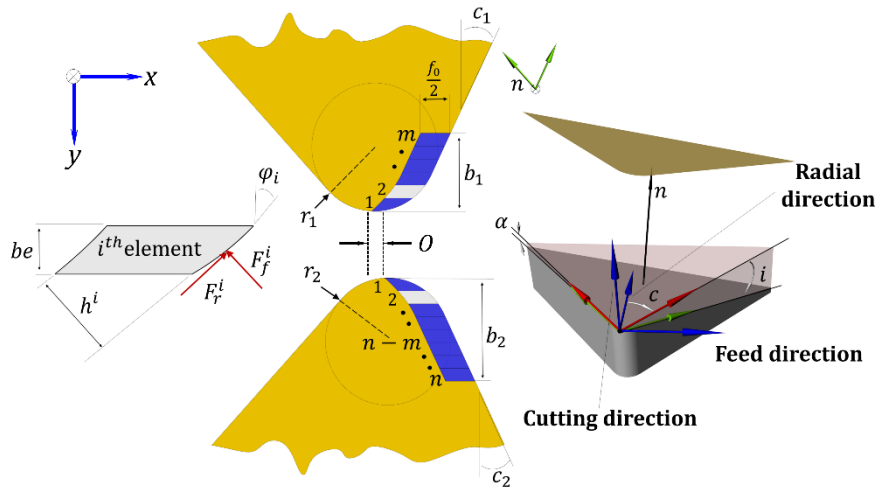
Figure 2.2. Modulated chip thickness on the tools having nose radius (r) and side edge cutting angle (C). A 3D view of the cutting insert. i, α and c are inclination, rake and side edge cutting angle, respectively. Elemental forces acting on an ith element located on the cutting edge of an insert.

In this configuration, feed velocity of the cutters must be the same. In addition to the identical feed velocity of the cutters, axial offset between the cutters should be equal to $O = (b_2 - b_1) \times tanC$ to make sure that cutting surface is shared and distributed equally over the tools, where b_2 and b_1 are depth of cuts for the second and the first cutters, respectively, and C is side edge cutting angle of the insert (see Figure 2.2). The axial

11

offset between the tools must be kept in the range of $0 \pm f_0/2$ not to violate the parallel cutting condition [25] where f_0 is feed velocity of the tools.

During cutting with tools having different side edge cutting angles, the cutting surface cannot be shared equally over the tools, and thus parallel operation condition cannot be met. Consequently, tools with different side edge cutting angle are not employed in this configuration. It is worth noticing that tools can cut a shared surface with different or identical depth of cuts. As will be further discussed in Chapter 3,parallel turning having tools with different depth of cuts is considered as a double-delay system while on the contrary, parallel turning with tools having similar depth of cut is a single-delay system.

2.2. Cutters cutting different surfaces

Another parallel turning operation in which two tools cut different surfaces is illustrated in Figure 2.3 and Figure 2.4. where the cutters can be mounted on different turrets or on the same one. There is no coupling between the cutters through the surfaces, however cutters can be coupled via structures, i.e. turret or workpiece.
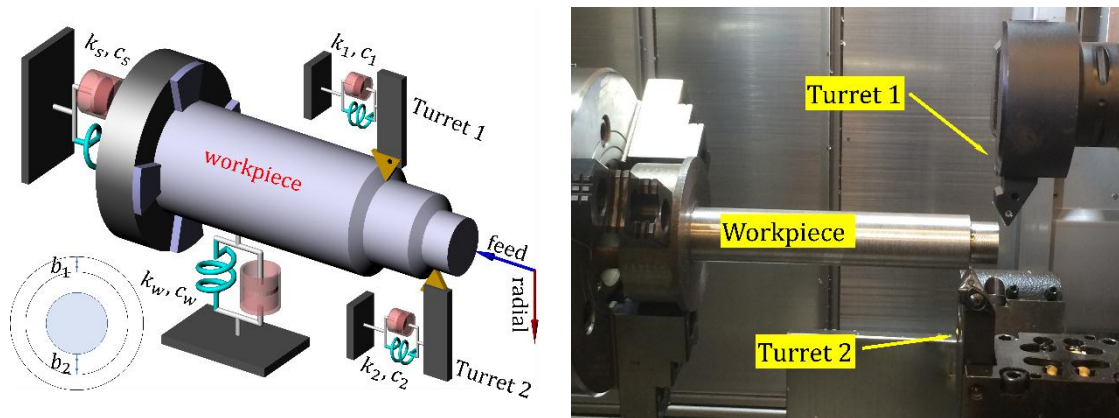
Figure 2.3. Cutters mounted on different turrets cutting different surfaces (Coupled via the workpiece dynamics)

To elaborate, during machining of a flexible workpiece with rigid tools, the only dynamic coupling between the cutters occurs due to the flexibility of the workpiece in the radial direction. Nonetheless, while machining a rigid workpiece with flexible tools which are installed on a single turret, dynamic coupling among the cutters is owing to the flexibility of the turret/tool holders structure in the radial direction.
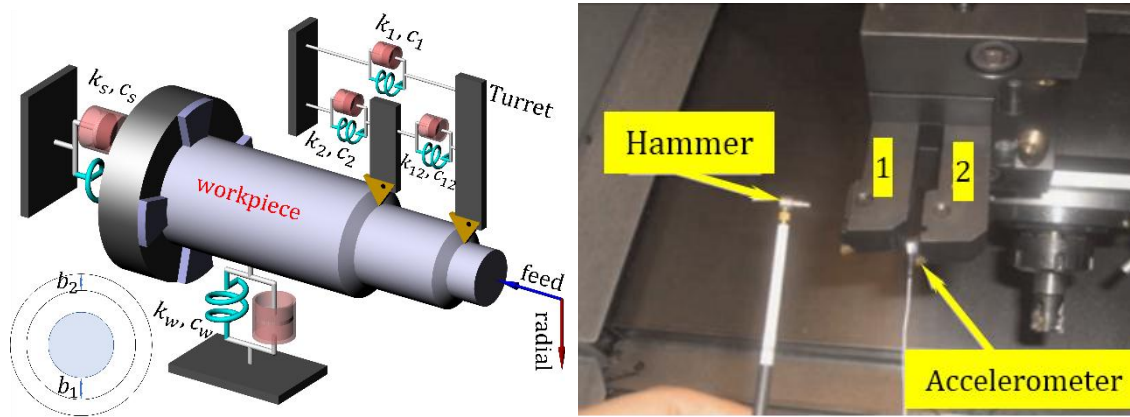
Figure 2.4. Cutters mounted on the same turret cutting different surfaces [31]
(Coupled via the turret structure)

Similar to the previous case, tools can have different or identical depth of cuts. Feed velocity of the cutters is set to be the same. However, unlike the previous case, tools having different side edge cutting angles can be utilized, and thus this additional geometry parameter can be adjusted properly for enhanced productivity.

In addition to mentioned configurations, there is two different types of tools/workpiece combination in the literature. Brecher et al. [26] (see Figure 2.5), investigated a parallel turning operation in which cutters can have radial alignment respect to each other. The results indicate that radial orientation of the tools when they are dynamically coupled, has prominent influence on increasing the chip removal rate. Hence, in addition to selecting spindle speed, radial angle between the cutters can be tuned to increase the productivity. Also. Reith et al. [32], developed an analytical formulation to chatter stability of a parallel turning having arbitrary number of cutters (see Figure 2.6). Despite the strong theoretical framework of the work presented in [32], to the author's knowledge, it is hard to implement the multi-cutter configuration in the industry since setting up the fixture seems to be complicated and it may rise obstacles to the machine operator to tune the cutters.
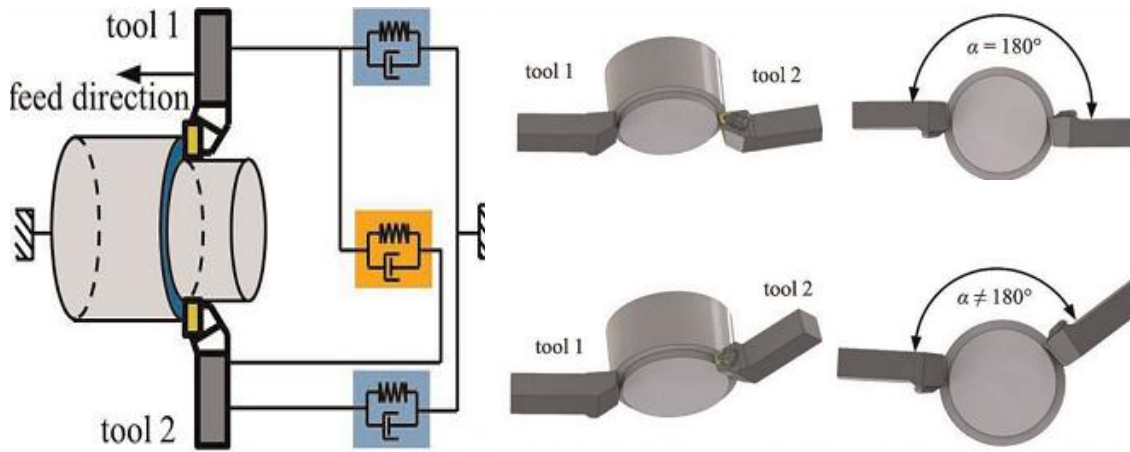
Figure 2.5. Dynamic coupling between the cutters and influence of radial angle on the delay between the cutters [26]
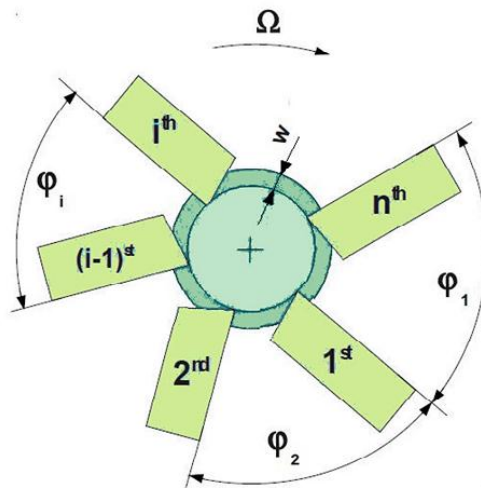
Figure 2.6. A schematic model for multi-cutter turning process [32]

Chapter 3 **DYNAMIC MODELLING AND PROCESS STABILITY**

A multi-dimensional model is presented and applied to two introduced configurations.

3.1.1. Dynamic Chip Thickness

In contrast with previously developed models for parallel turning [25-26], [29-35], the current study considers effects of side edge angle and nose radius in different parallel turning strategies. To describe the chip geometry of an insert in the nose region, the area must be divided into smaller trapezoid-like elements [28], as illustrated by Figure 2.2. Geometrical parameters describing each element in the nose region, i.e. the elemental depth of cut (b_e) and side edge cutting angle of each element (φ_i) were introduced in [28]. The modulated chip thickness and forces parallel and perpendicular to the cutting edge of the element must be projected in the global coordinates of the CNC machine. As far as cutting depth on each tool is different, two different regions describe the cutting process. In the first region, the depth of b_1 is removed by the first and second tools simultaneously. In the second region, on the other hand, the cutting depth of b_2-b_1 is solely cut by the second tool. In each of these regions a different time delay exists, presenting a double-delay system. In the former region, the vibrating cutting edge of a tool removes the surface generated by the other tool at a half rotation period before. Thus, the delay in this region is equal to $\tau/2$. Moreover, the static part of the chip thickness which is shared evenly between the cutters is equal to feed per revolution. Then, the total chip thickness for each element on the tool can be written as a summation of regenerative and static parts of the chip thickness as follows:

$$h_{c_1}^i(t) = \frac{f_s}{2}\cos C_1 + \Delta y_{12}\sin\varphi_{i,c_1} + \Delta x_{12}\cos\varphi_{i,c_1}, \qquad i = 1, m$$

$$h_{c_2}^j(t) = \frac{f_s}{2}\cos C_2 + \Delta y_{21}\sin\varphi_{j,c_2} + \Delta x_{21}\cos\varphi_{j,c_2}, \qquad j = n-m, n$$

(1)

where Δx_{12} and Δy_{12} are given by:

$$\Delta y_{12} = y_{c_1}(t) - y_{c_2}\left(t - \frac{\tau}{2}\right) - y_w(t) + y_w\left(t - \frac{\tau}{2}\right)$$

$$\Delta x_{12} = x_{c_1}(t) - x_{c_2}\left(t - \frac{\tau}{2}\right) - x_w(t) + x_w\left(t - \frac{\tau}{2}\right)$$

(2)

where Δx_{21} and Δy_{21} can be defined similarly. In the latter region, however, vibrating edge of the second tool cuts the surface left by the same tool from one revolution before, and thus the delay in this region is equal to τ. Furthermore, the static part of the chip thickness is equal to the feed per revolution. Therefore, the total chip thickness in the second region can be expressed as follows:

$$h_{c_2}^j(t) = f_s \cos C_2 + \Delta y_{22} \sin \varphi_{j,c_2} + \Delta x_{22} \cos \varphi_{j,c_2}, \qquad j = 1, n - m - 1 \tag{3}$$

where:

$$\Delta y_{22} = -y_{c_2}(t) + y_{c_2}(t - \tau) + y_w(t) - y_w(t - \tau)$$
$$\Delta x_{22} = x_{c_2}(t) - x_{c_2}(t - \tau) - x_w(t) + x_w(t - \tau) \tag{4}$$

Although, one may consider the dynamic vibration of the cutters or the workpiece in either positive or negative direction, dynamic chip thickness definition must remain unchanged. For example, based on the coordinate system shown in the Figure 2.2, the current dynamic displacement of the first cutter in the positive x direction increases the chip thickness of the first tool while dynamic displacement of the second tool at half revelation before in positive x direction decreases the chip thickness of the first tool. Same rule should be applied to form the dynamic chip thickness.

In equations (1-4), y and x represent the cutter and workpiece displacements in radial and feed directions, respectively. t and τ are time and period of rotation, respectively. Furthermore, f_s and C are the feed per revolution and side edge angle of the cutting tool, respectively. Finally, n and m are the number of elements used in meshing of the second and the first tool, respectively. As aforementioned, if the cutting depths on each tool are identical, the only delay in the process is $\tau/2$, the parallel turning operation is a single-delay system. In this case, the dynamic chip thickness on each of the tools can be presented as follows:

$$h_{c_1}^i(t) = \frac{f_s}{2} \cos C_1 + \Delta y_{12} \sin \varphi_{i,c_1} + \Delta x_{12} \cos \varphi_{i,c_1}, \qquad i = 1, m$$

$$h_{c_2}^j(t) = \frac{f_s}{2} \cos C_2 + \Delta y_{21} \sin \varphi_{j,c_2} + \Delta x_{21} \cos \varphi_{j,c_2}, \qquad j = 1, m \tag{5}$$

where Δx_{12} and Δy_{12} are given by:

$$\Delta y_{12} = y_{c_1}(t) - y_{c_2}\left(t - \frac{\tau}{2}\right) - y_w(t) + y_w\left(t - \frac{\tau}{2}\right)$$

$$\Delta x_{12} = x_{c_1}(t) - x_{c_2}\left(t - \frac{\tau}{2}\right) - x_w(t) + x_w\left(t - \frac{\tau}{2}\right)$$

(6)

where Δx_{21} and Δy_{21} can be defined similarly.

3.1.2. Dynamic Cutting Forces

By summing the transformed forces acting on each element on the cutting edge of the insert, the total forces in feed and radial direction, $\overline{F_x}, \overline{F_y}$, can be calculated as follows:

(7)

$$\left\{\begin{matrix} \overline{F_x} \\ \overline{F_y} \end{matrix}\right\}_{c_1} = b_{e_1} \sum_{i=1}^{m} \left([T_{c_1}^i][C_{c_1}][D_{c_1}^i]\right)\left\{\begin{matrix} \Delta x_{12} \\ \Delta y_{12} \end{matrix}\right\}$$

$$\left\{\begin{matrix} \overline{F_x} \\ \overline{F_y} \end{matrix}\right\}_{c_2} = b_{e_2} \sum_{j=1}^{n-m-1} \left([T_{c_2}^j][C_{c_2}][D_{c_2}^j]\right)\left\{\begin{matrix} \Delta x_{22} \\ \Delta y_{22} \end{matrix}\right\} + b_{e_1} \sum_{j=n-m}^{n} \left([T_{c_2}^j][C_{c_2}][D_{c_2}^j]\right)\left\{\begin{matrix} \Delta x_{21} \\ \Delta y_{21} \end{matrix}\right\}$$

where $[D_{c_1}^i]$ and $[D_{c_2}^j]$ project the chip thickness onto the global coordinates, $[C_{c_1}]$ and $[C_{c_2}]$ represent the force coefficient matrix and b_e is the width of each element. Matrices $[T_{c_1}^i]$ and $[T_{c_2}^j]$ transform the forces acting upon the cutting edges onto the feed and radial directions.

3.1.3. Stability Analysis using Frequency Domain Solution

Dynamic displacements of the system, x_p, y_p, can be determined by using dynamic cutting forces, $\overline{F_x^p}, \overline{F_y^p}$, and dynamic transfer functions as follows [13]:

(8)

$$\left\{\begin{matrix} x_p(t) \\ y_p(t) \end{matrix}\right\} = \begin{bmatrix} G_{xx}^p & G_{xy}^p \\ G_{yx}^p & G_{yy}^p \end{bmatrix}\left\{\begin{matrix} \overline{F_x^p}(t) \\ \overline{F_y^p}(t) \end{matrix}\right\} \quad , \quad p: c_1, c_2, w$$

It should be noted that considering the geometry of most turning processes the tools can be assumed to be flexible in the feed direction whilst the workpiece is flexible in the radial direction only. Hence, cross transfer functions can be neglected in the calculations. Marginal stability is obtained when the real part of the characteristic equation is zero and the system oscillates with a constant amplitude at the chatter frequency of ω_c [36]. Therefore, the dynamic displacements and forces can be expressed as follows:

17

$$\{x, y\}_p \, e^{i\omega_c t} = \left[G_{x,y}^p \right] \left\{ \overline{F_{x,y}^p} \right\} e^{i\omega_c t} \qquad p : c_1, c_2, w \tag{9}$$

Equation (9) represents six equations for the displacements of cutter 1, cutter 2 and workpiece in the feed and radial directions. However, since it is assumed that cutters never lose their contact with workpiece, equations pertaining to the workpiece's displacements can be written in terms of cutters' displacement as follows [15]:

$$x_w e^{i\omega_c t} = G_{xx}^w \left(\overline{F_x^{c_1}} + \overline{F_x^{c_2}} \right) e^{i\omega_c t} \tag{10}$$

$$y_w e^{i\omega_c t} = G_{yy}^w \left(\overline{F_y^{c_1}} - \overline{F_y^{c_2}} \right) e^{i\omega_c t}$$

Substituting equations (9-10) in equation (7), and re-arranging them in a single matrix form [15], the global dynamic force matrix becomes:

$$\begin{Bmatrix} \overline{F_x^{c1}} \\ \overline{F_y^{c1}} \\ \overline{F_x^{c2}} \\ \overline{F_y^{c2}} \end{Bmatrix} e^{i\omega_c t} = \left(b_{e_1} \left[\overline{A_1}(m,n) \right] \left[\overline{G}_1(i\omega_c, \tau) \right] + b_{e_2} \left[\overline{A_2}(m,n) \right] \left[\overline{G}_2(i\omega_c, \tau) \right] \right) \begin{Bmatrix} \overline{F_x^{c1}} \\ \overline{F_y^{c1}} \\ \overline{F_x^{c2}} \\ \overline{F_y^{c2}} \end{Bmatrix} e^{i\omega_c t} \tag{11}$$

Matrices in equation (11) are as follows:

$$\overline{A_1}(m,n) = \begin{bmatrix} \sum_{i=1}^{m} [T_{c_1}^i][C_{c_1}][D_{c_1}^i] & [0_{2\times2}] \\[2em] [0_{2\times2}] & \sum_{j=n-m}^{n} [T_{c_2}^j][C_{c_2}][D_{c_2}^j] \end{bmatrix}, \tag{11-1}$$

$$\overline{A_2}(m,n) = \begin{bmatrix} [0_{2\times2}] & [0_{2\times2}] \\[1.5em] [0_{2\times2}] & \sum_{j=1}^{n-m-1} [T_{c_2}^j][C_{c_2}][D_{c_2}^j] \end{bmatrix}$$

Also

$$\overline{G}_1 = \begin{bmatrix} G_{xx}^{c_1} + G_{xx}^w R & 0 & -G_{xx}^{c_2} e^{-i\omega_c \frac{\tau}{2}} + G_{xx}^w R & 0 \\[1em] 0 & G_{yy}^{c_1} + G_{yy}^w R & 0 & -G_{yy}^{c_2} e^{-i\omega_c \frac{\tau}{2}} - G_{yy}^w R \\[1em] -G_{xx}^{c_1} e^{-i\omega_c \frac{\tau}{2}} + G_{xx}^w R & 0 & G_{xx}^{c_2} + G_{xx}^w R & 0 \\[1em] 0 & G_{yy}^{c_1} e^{-i\omega_c \frac{\tau}{2}} - G_{yy}^w R & 0 & -G_{yy}^{c_2} + G_{yy}^w R \end{bmatrix} \tag{11-2}$$

and

18

$$\bar{G}_2 = \begin{bmatrix} 0 & 0 & 0 & 0 \\ 0 & 0 & 0 & 0 \\ -G_{xx}^w R' & 0 & G_{xx}^{c2} R' - G_{xx}^w R' & 0 \\ 0 & -G_{yy}^w R' & 0 & G_{yy}^w R \end{bmatrix} \tag{11-3}$$

where $R = 1 - e^{-i\omega_c \tau/2}$, $R' = 1 - e^{-i\omega_c \tau}$.

Equation (11) has nontrivial solution if the determinant of the following characteristic equation is zero:

$$E = \det\left[I_{4\times4} - \left(b_{e_1}\left[\overline{A_1}(m,n)\right]\left[\overline{G}_1(i\omega_c,\tau)\right] + b_{e_2}\left[\overline{A_2}(m,n)\right]\left[\overline{G}_2(i\omega_c,\tau)\right] \right) \right] = 0 \tag{12}$$

where I is the 4×4 identity matrix. Since Equation (12) is a complex one its real and imaginary parts must be set to zero:

$$R\{E(b_{e_1},\omega_c,\Omega,m,n)\} = 0 \tag{13}$$
$$I\{E(b_{e_1},\omega_c,\Omega,m,n)\} = 0$$

where $\Omega = 60/\tau$ is the spindle rotation period. For the current configuration, before proceeding to the stability calculations, three parameters must be chosen initially. Firstly, depth of cut of the second tool, (b_2), and secondly, the number of elements which mesh the nose region of the first and second cutter, (m_{nose}, n_{nose}), respectively. For the sake of simplicity, m_{nose} and n_{nose} are selected in a way that the depth of each element for both tools is equal, i.e. $b_{e_1} = b_{e_2}$. As the next step, the total number of elements in the second tool, i.e. $n = b_2/b_{e_1}$, can be determined. Finally, the number of elements which are in cut on the first tool, i.e. m, can be calculated by solving the eigenvalue problem iteratively. Multi-Dimensional Bisection Method (MDBM) [37-38], provides a fast and efficient algorithm to locate the roots of Equation (13). Similar with proposed solution in [28], it should be noted that the presented solution (see Equations. (12) and (13)) determines the elemental stability limit, (b_{e_stable}), which is the stability limit of an element in the cutting edge of the first tool. Hence, the total stability limit of the tool should be computed by multiplying the number of elements in the cut by the elemental stability limit, i.e. $m \times b_{e\_stable}$. In order to achieve the elemental stability limit using MDBM, firstly, an appropriate range and incremental step for the chatter frequency, ω_c, spindle speed, Ω, and elemental depth of cut, w, must be selected. Matrices $\overline{A_1}$ and $\overline{A_2}$ are calculated for one element engagement of the first cutter. Later, the elemental stability limit is computed

19

by solving equation (13). In the next step, it should be checked if calculated stability limit ($m \times b_{e\_stable}$) is inside the part of the cutter edge considered in the calculation of eigenvalue problem.

$$\left(m-1\right)b_{e_1} < m\left\{b_{e\_stable}\right\} < mb_{e_1}$$
$$mb_{e_1} < m\left\{b_{e\_stable}\right\} < \left(m-1\right)b_{e_1}$$

(14)

If condition stated in Equation (14) is not met, another element will be added and the same procedure will be repeated until the determined stability limit satisfied equation (14). It should be noted that large number of meshes in the nose region of the tools will further enhance the accuracy of the simulations at the expense of solution time.
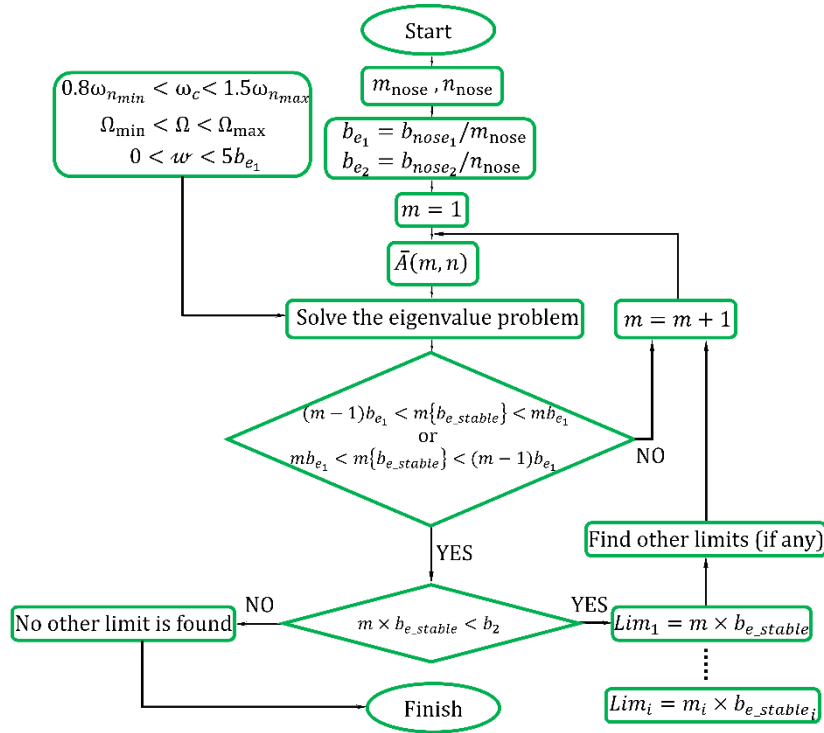
Figure 3.1. Flowchart used to calculate the stability limits.

Figure 3.1 displays the procedure of determining stability limits in a flowchart. In the formulations, it is assumed that b_2 is equal and bigger than b_1, and thus those b_1 values which are smaller than b_2 are acceptable solutions. However, to complete the stability map for $b_1 > b_2$ values, tools' or workpiece contact points' dynamics must be swapped in the simulations and then calculated b_2 for given b_1 can be plotted in the same map.

3.1.4. Time Domain Model

Created forces during cutting process will cause vibrating the tools and workpiece. Subsequently, the modulated dynamic chip thickness of the tools will be influenced by the dynamic properties of the system. Since the cutting forces depend on dynamic chip thickness, modulated chip thickness in current revolution of cut will be affecting the cutting forces in the next revolution. The governing delayed differential equation (DDE) of the system can be modeled (see Figure 3.2) in MATLAB/Simulink [39] as a closed loop block diagram [26], [35-36]. Even though inclusion of the static chip thickness and edge forces in the time domain model will not influence the stability boundaries, it leads to predict accurate force and displacement values in the simulations. It is worth noticing that step size must be selected small enough in order to have sufficient simulation points in each chatter wave [25]. Runga-Kutta method [40] was used to solve the DDE.
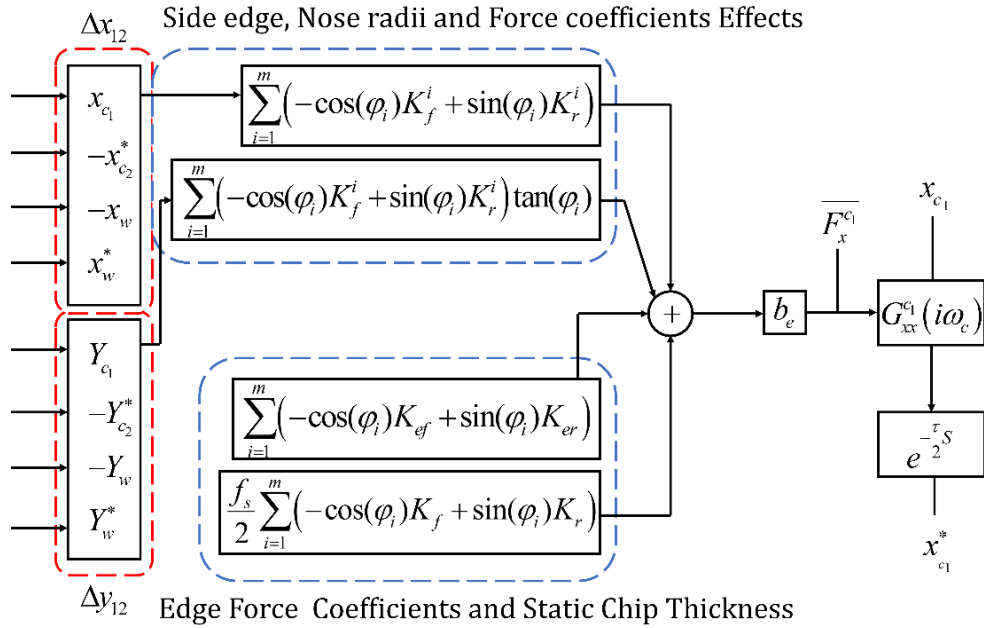
Figure 3.2. Time domain block diagram to simulate the dynamic chip thickness of the first cutter.

In order to illustrate the time domain approach, dynamic displacements of the first cutter in the feed direction, which depend on dynamic displacement of second cutter and workpiece in both radial and feed directions, calculated in the Simulink environment and are given in Figure 3.2. The same procedure must be applied to determine the dynamic displacements of other components, i.e. cutter 1, 2 and the workpiece, in the

radial and feed directions. Thereafter, the displacements and delayed displacements must be feedbacked to corresponding block diagrams ($\Delta x_{12}, \Delta y_{12}, \Delta x_{21}, \Delta y_{21}$) in accord with the definition of the dynamic chip thickness (see Equations (1-4)).

3.2.   Two Cutters Cutting Different Surfaces

Another parallel turning operation in which two tools cut different surfaces has been illustrated in Figure 3.3. The cutters can be mounted on different turrets or can be mounted on a single turret. In this configuration in which one of the tool is performing roughing and the other one finishing operation is widely being used in industry. In case the tools are cutting different surfaces, similar with the first case, feed velocity of the cutters set to be the same. Nevertheless, in contrast with the first case, tools having different side edge cutting angles could be utilized. To develop stability formulation, same procedure as it discussed in the first case should be followed.

(a)   (b)

Figure 3.3. Tool cutting different surfaces, (a) on different turrets, (b) on the same turret

The total chip thickness for the cutters are given by:

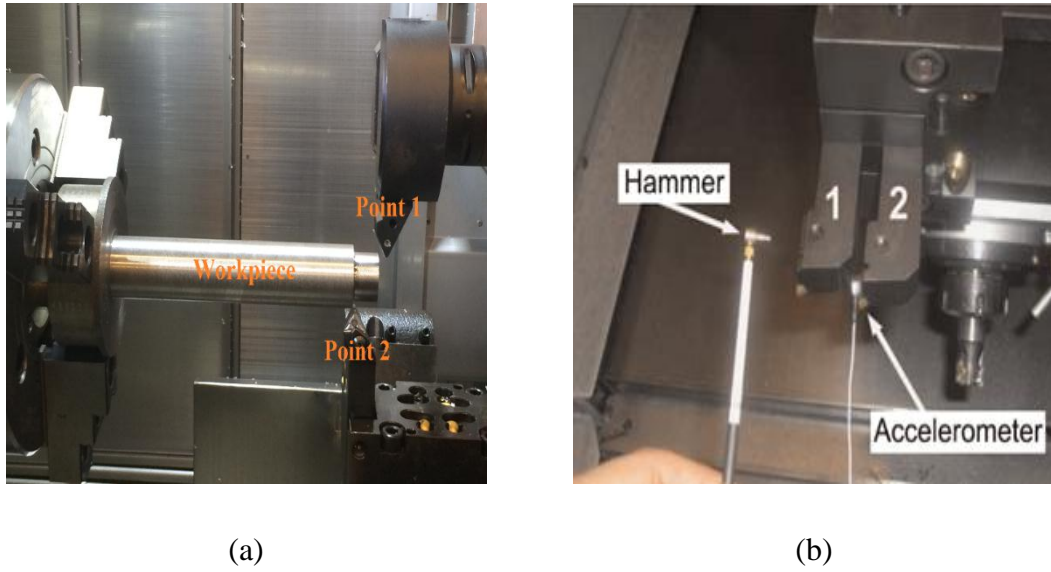$$h_{c_1}^{i}(t) = f_s \cos k_1 + \Delta y_{11} \sin \varphi_i + \Delta x_{11} \cos \varphi_i, \qquad i = 1, m \tag{15}$$
$$h_{c_2}^{j}(t) = f_s \cos k_2 + \Delta y_{22} \sin \varphi_j + \Delta x_{22} \cos \varphi_j, \qquad j = 1, n$$

Where:

$$\Delta y_{11} = y_{c_1}(t) - y_{c_1}(t-\tau) - y_{w_1}(t) + y_{w_1}(t-\tau)$$

$$\Delta x_{11} = x_{c_1}(t) - x_{c_1}(t-\tau) - x_{w_1}(t) + x_{w_1}(t-\tau)$$

$$\Delta y_{22} = -y_{c_2}(t) + y_{c_2}(t-\tau) + y_{w_2}(t) - y_{w_2}(t-\tau)$$

$$\Delta x_{22} = x_{c_2}(t) - x_{c_2}(t-\tau) - x_{w_2}(t) + x_{w_2}(t-\tau)$$

(16)

Indices 1 and 2 shows the contact points of the cutters. Similar with previous case formulation, total dynamic forces exerting on the tools in the general coordinate should be expressed in terms of dynamic transfer functions and dynamic displacement of the system's component. By employing the extracted equations, and manipulating them algebraically to transform into a single matrix form, the following is obtained:

$$\left\{ \begin{matrix} \overline{F_x^{c1}} \\ \overline{F_y^{c1}} \\ \overline{F_x^{c2}} \\ \overline{F_y^{c2}} \end{matrix} \right\} e^{i\omega_c t} = \left[\overline{A}(m,n) \right] \left[\overline{G}(i\omega_c,\tau) \right] \left\{ \begin{matrix} \overline{F_x^{c1}} \\ \overline{F_y^{c1}} \\ \overline{F_x^{c2}} \\ \overline{F_y^{c2}} \end{matrix} \right\} e^{i\omega_c t}$$

(17)

Where

$$\overline{A}(m,n) = \begin{bmatrix} \sum_{i=1}^{m} [T_{c_1}^i][C_{c_1}][D_{c_1}^i] & [0_{2\times2}] \\ [0_{2\times2}] & \sum_{j=1}^{n} [T_{c_2}^j][C_{c_2}][D_{c_2}^j] \end{bmatrix}$$

(18)

and

$$\overline{G}_1 = \begin{bmatrix} b_{e_1}\left(G_{xx}^{c_{1,1}} - G_{xx}^{w_{1,1}}\right) & 0 & b_{e_1}\left(G_{xx}^{c_{2,1}} - G_{xx}^{w_{2,1}}\right) & 0 \\ 0 & b_{e_1}\left(G_{yy}^{w_{1,1}} + G_{yy}^{c_{1,1}}\right) & 0 & -b_{e_1}\left(G_{yy}^{w_{2,1}} + G_{yy}^{c_{2,1}}\right) \\ b_{e_2}\left(G_{xx}^{c_{1,2}} - G_{xx}^{w_{1,2}}\right) & 0 & b_{e_2}\left(G_{xx}^{c_{2,2}} - G_{xx}^{w_{2,2}}\right) & 0 \\ 0 & -b_{e_2}\left(G_{yy}^{w_{1,2}} + G_{yy}^{c_{1,2}}\right) & 0 & b_{e_2}\left(G_{yy}^{w_{2,1}} + G_{yy}^{c_{2,1}}\right) \end{bmatrix}$$

(19)

The equation 17 has nontrivial solution if the determinant of the following equation is zero:

$$E = \det\left[I_{4\times4} - \left(1 - e^{-i\omega_c \tau}\right)\left[\overline{A}(m,n) \right]\left[\overline{G}(i\omega_c,\tau) \right] \right] = 0$$

(20)

The solution method will be the same as the first case. Moreover, time domain simulation can be easily adapted from the first case diagrams, in accord with definition provided dynamic chip thickness for second case.

23

Chapter 4 **SIMULATIONS AND EXPERIMENTAL RESULTS**

In order to discuss the chatter stability solutions of parallel turning obtained from frequency and time domain simulations, two different configurations with flexible tools and workpiece combinations (four cases in total) are investigated and verified experimentally. Modal parameter were derived from fitted curves to tap testing results [36] (Figure 4.1). In experiments, sound spectrum was measured and image of surface was taken in order to detect chatter. The force coefficients were calibrated mechanistically based on linear edge force model [41]. In each case, effects of the nose radius and the side edge cutting angle of the inserts on the stability are investigated and a methodology for proper selection of the process parameters is presented to enhance productivity in each configuration. The simulation and experimental results proved that by setting the depth of cuts of the tools in the parallel turning mode bellow the tools' critical depth in single turning mode a chatter-free process can be achieved. However, the maximum stable MRR in each case can happen on different points of the stability map.

4.1.   Cutting a Shared Surface

4.1.1. Flexible Workpiece

This set of experiments is conducted to observe the chatter stability of a parallel turning operation while cutting a shared surface of a flexible workpiece. Tools are clamped in a way to achieve the maximum stiffness in the feed direction. The workpiece and insert properties are given in Table 1. The workpiece was machined by SECO TNMG TP2501 inserts on a Mori Seiki NT CNC machine.

Table 1. Workpiece and process and geometry parameters [case 1]

Workpiece material	AISI 1050	Feed cutting force Coefficient K_{fc}	692 MPa
Workpiece diameter	42 mm	Feed edge force Coefficient K_{fe}	148 N/mm
Workpiece length	127 mm	Radial cutting force Coefficient K_r	178 MPa
nose radius r	0.4 mm	Radial edge force Coefficient K_{re}	18 N/mm
side edge angle C	30°	Feed velocity f_0	0.1 mm/rev
inclination angle	5°	Spindle speed Ω	1550 RPM
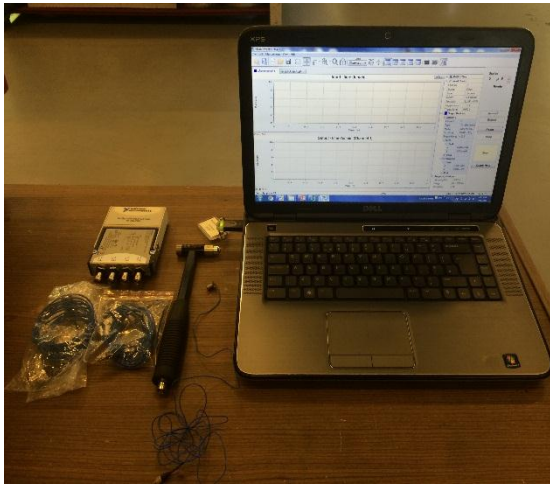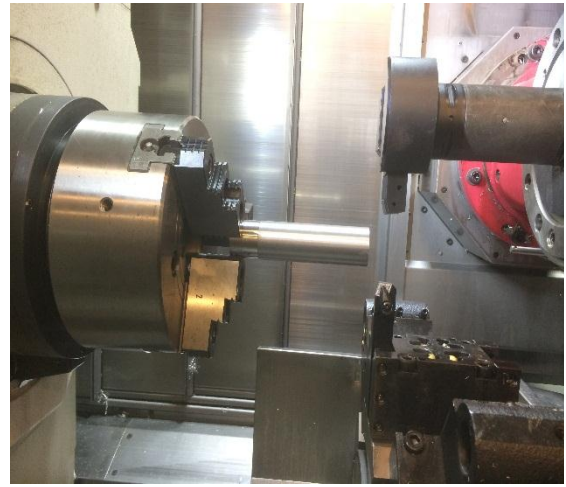
(a)   (b)

Figure 4.1. Tap testing measurement and CutPro [36] (a). Parallel turning operation(b)

A major problem in chatter tests involving a flexible workpiece is its varying dynamic properties. In order to minimize the effect of dynamic properties variation, the cut length, i.e. the part where the diameter is reduced, is kept very short in comparison with the total length of the workpiece. Additionally, two identical workpieces were used to complete the stability tests. This was verified by the measured modal data of the workpiece which showed negligible variation before and after the cut. Modal data of the workpiece before and after the cut is presented in Table 2

Table 2, Modal data of the workpiece [case 1]

Component	f_n(Hz)	Stiffness(N/m)	Damping (%)
Workpiece (Before Cut)	538	1.2×10^7	1.7
Workpiece (After Cut)	575	1.28×10^7	1.52
Tool 1	3434	1.45×10^9	0.7
Tool 2	4020	1.93×10^8	2.29

Stability map for this case is generated by both frequency and time domain simulations, and verified experimentally as shown in Figure 4.2.a. The absolute stability limit of the tools for single tool operation mode is calculated as 0.84 mm using the model presented in [28]. The stability boundaries in parallel turning of a flexible workpiece forms an area separating the stable and unstable points for different depth of cuts. In a parallel operation, if the depth of cut of each tool is smaller than the stability limit of the same tool in the single tool operation, an individual upper limit for stable region exists since the lower stable limit is zero. By setting higher depth of cut values than the critical limit of the single tool turning, lower limit of stability map becomes non-zero, and thus system is transformed into a new stability region having upper and lower stability limits. By increasing b_2, lines of lower and upper stable limit for b_1 increase proportionally parallel with line $b_2 = b_1$. As it can be seen in Figure 4.2.a, the difference between the lower and upper stable limits for b_1, when b_2 is bigger than 0.84 mm is about 0.75 mm which is almost equal to the stability limit of the single tool turning. In fact, a stable process can be approached where difference between the cutters' depth of cut is less than the stable depth of cut of the cutters in single tool turning. In plainer words, total required radial force to initiate chatter instability are equal in both parallel and single turning.

On the line $b_2 = b_1$, from theoretical stand point, the dynamic forces acting on the workpiece in the radial direction should have exactly the same magnitude due to the identical nose radii, force coefficients, tool dynamics and depth of cut, and thus cancelling each other in this direction. Furthermore, since both tools are assumed to be rigid, theoretically the stability limits reach infinity.
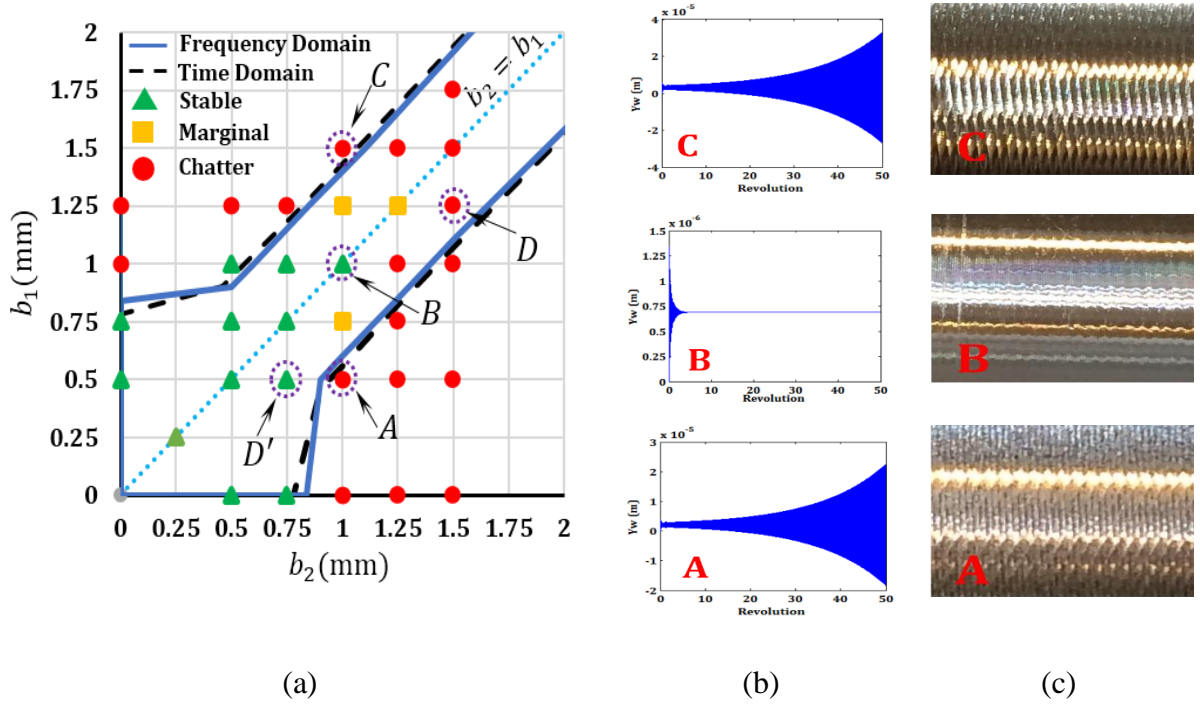
Figure 4.2. (a) Stability map predicted by frequency solution and time domain model at 1550 RPM. (b) Dynamic chip thickness for three different points at b_2=1mm. (c) Chatter marks left on the surface in stable and unstable processes.

In order to observe the stability behavior of the system experimentally, the second cutter's depth of cut is set to 1mm, and for three b_1 values (0.5,1 and 1.5 mm) dynamic displacement of the workpiece is simulated in the time domain and illustrated in Figure 4.2.b. The generated surfaces after the tests for three different depths of cuts are shown in Figure 4.2.c. As it is clear from the time domain simulations and the resulting surfaces, point A and C are unstable cases whereas B is a stable one.

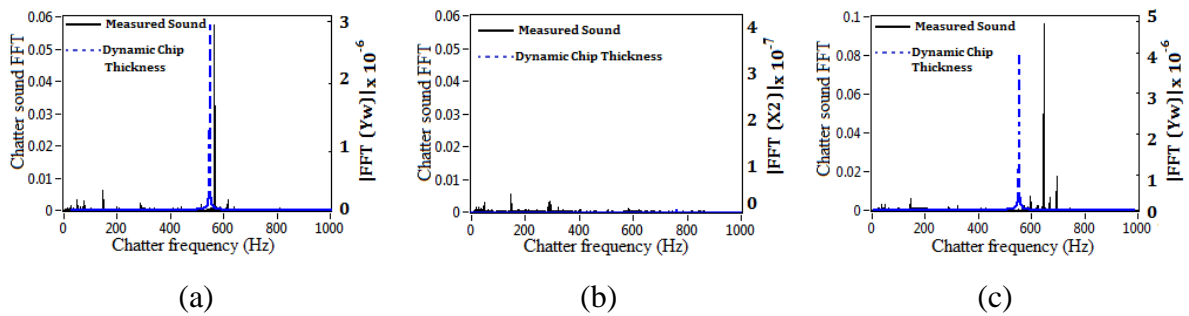Figure 4.3. Frequency spectrums of the measured sound and dynamic displacements of the workpiece simulated in the time domain for points (a) A, (b) B and (c) C.

In Figure 4.3, the spectrums of the sound measured during the experiments for points A, B and C are compared with the spectrums of the simulated dynamic displacements of the workpiece in time domain. At point C, because of the material removal from the

workpiece, natural frequency increased slightly causing the chatter frequency to be higher than the one for point A.

Even though there are some differences between the simulation and experimental results, the overall trends are similar. The discrepancies may root in the difference between the force coefficients of the upper and lower tools. To elaborate, sensitivity of the stability limit to variation of cutting force coefficients is demonstrated by an example case illustrated in Figure 4.4. The force coefficients for two tools may not be exactly the same due to slight differences in insert or tool holder geometries resulting in different nose and edge hone radii as well as rake or inclination angles owing to manufacturing tolerances of these features. According to the calculated stability limit, point D and D' in Figure 4.2.a lie within the stable area boundaries. However, in the experiments, point D found to be unstable. Figure 4.4 demonstrates the dynamic displacement of the workpiece, calculated in the time domain, for 50 revolutions for points D and D' based on new sets of force coefficients. It can be seen from the figure that even less than 10 percent change in cutting force coefficients of the tools, can change a stable cut to an unstable one for relatively higher depth of cuts, i.e. point D, due to the higher unbalanced forces in the radial directions. However, point D' still remains in the stable condition due to smaller depth of cut, and thus smaller unbalanced forces in the radial direction.

(a) (b)
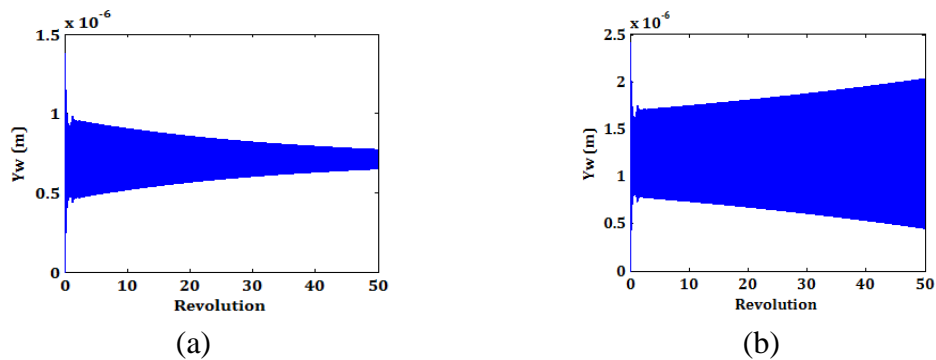
Figure 4.4. Effect of 10% change in the force coefficient of the first tool (Kf_1=760MPa, Kr_1=196Mpa) on the stability limit. (a) Point D' stable process, (b) Point D unstable process.

In accord with the fact that radial forces are countering each other in parallel turning of the shared surface of a flexible workpiece, employing geometrically and mechanically identical cutters, will lead to improved productivity. Intuitively, in the current configuration, line $b_1 = b_2$ provide the maximum productivity.

Insert's nose radius and side edge cutting angle affect the stability map in parallel turning operation. Generally, increasing the nose radius and/or side edge cutting angle lead to increased projected resultant forces in the radial directions and decreased forces in the feed direction. By increasing the nose radii to 1.2 mm (see Figure 4.5.a.), and side edge angle to 35° (see Figure 4.5.b.) contribution of workpiece's dynamics drastically increases leading to extremely shrunk stability maps.

(a)   (b)

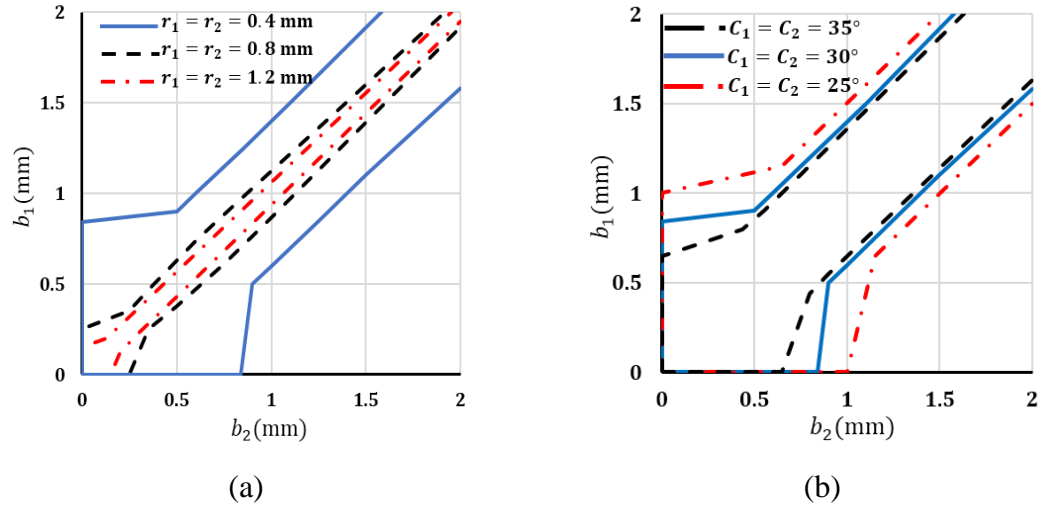Figure 4.5. Variation of stability map with different nose radius values ($C_1 = C_2 = 30°$) (a) and side edge cutting angles ($r_1 = r_2 = 0.4\ mm$) (b) at 1550 RPM.

4.1.1. Flexible Tools

This set of experiments was carried out to verify the proposed stability model for flexible tools/rigid workpiece combination in parallel turning. A relatively rigid workpiece was cut with SECO CNMG TP2501 insert on a Mori Seiki NT CNC machine. The workpiece and insert properties are tabulated in Table 3. The modal data measured in the tap testing are listed in Table 4.

Table 3. Workpiece and process and geometry parameters for Case 2.

Workpiece material	1050 steel	Feed cutting force Coefficient K_{fc}	681 MPa
Workpiece diameter	75 mm	Feed edge force Coefficient K_{fe}	119 N/mm
Workpiece length	100 mm	Radial cutting force Coefficient K_{rc}	184 MPa
nose radius r	0.4 mm	Radial edge force Coefficient K_{re}	14 N/mm
side edge angle C	15°	Feed velocity f_0	0.1 mm/rev
inclination angle	6°	Spindle speed Ω	1500 RPM

Table 4. Modal data of the tools and workpiece in Case 2.

Component	Mode	f_n(Hz)	Stiffness(N/m)	Damping (%)
Workpiece	1	756	2.308×10^8	2.4
Tool 1	1	1178.6	1.354×10^7	1.5
Tool 2	1	1452.3	2.411×10^7	1.1

Absolute stability limits of the cutters are calculated as 0.82 and 1 mm for the first and second cutter in single tool turning operation mode using the model presented in [28]. In the next step, absolute stability limit of the first tool in parallel turning was determined for different depth of cut values of the second tool and illustrated by Figure 4.6.a. Interestingly, by further increasing the depth of cut of each cutter beyond its stable limit in single mode turning, the process may still remain stable [25]. To illustrate, by increasing b_2 beyond 1 mm, the cutting process for small values of b_1 is unstable. However, by further increasing b_1, the system enters a stable region, and finally leaves the stable region and remains unstable. Similar to the frequency domain solution, the time domain simulations indicate the same stability behavior with multiple regions.

(a) *(b)* *(c)*
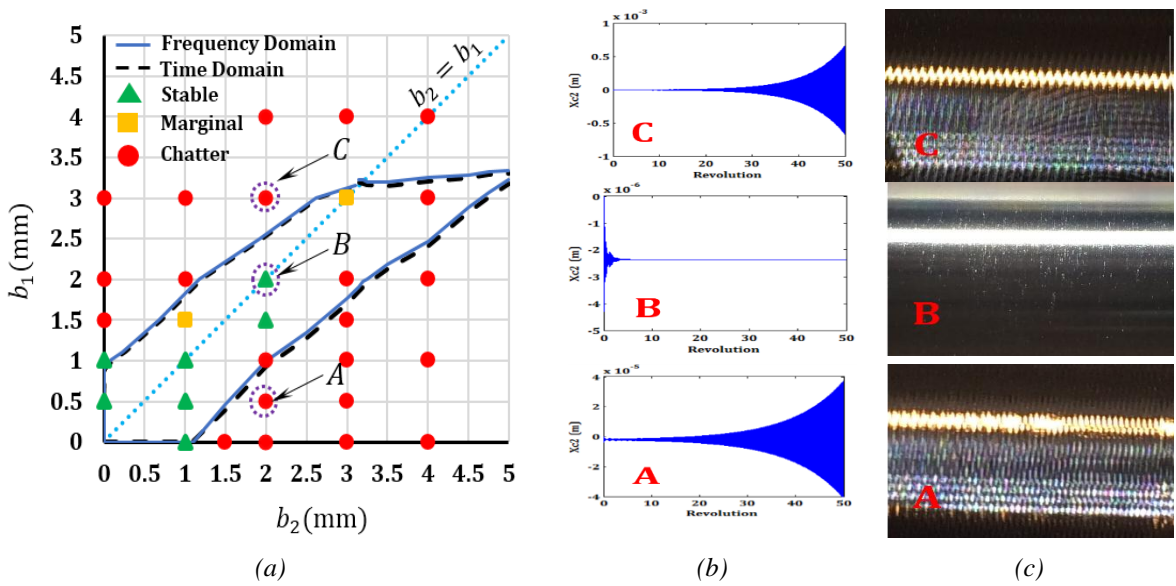
Figure 4.6. (a) Stability map predicted by frequency solution and time domain model at 1500 RPM. (b) Dynamic chip thickness for three different b_1 points where b_2=2mm. (c) Chatter marks left on the surface in stable and unstable processes.

To illustrate this, three values for b_1 (0.5, 2 and 3mm) are selected for a given b_2=2mm and the simulated dynamic chip thickness of the second tool are displayed in Figure 4.6.*b*. Additionally, chatter marks can be seen on the workpiece for the unstable cases (A and

C) whereas the generated surface is remarkably smooth for the stable process (B) as shown in Figure 4.6.c.

Sound spectrum of the experimental points A and C were measured by a microphone and compared with FFT of the dynamic chip thickness of the second tool in the time domain simulations. For cases A and C, the chatter frequencies (1475 and 1220 Hz) are close to the second and the first cutter's natural frequencies, i.e. 1452.3 and 1176.6 Hz, respectively (see Figure 4.7). Predicted stable boundaries in frequency and time domain unanimously agree with the experimental results.
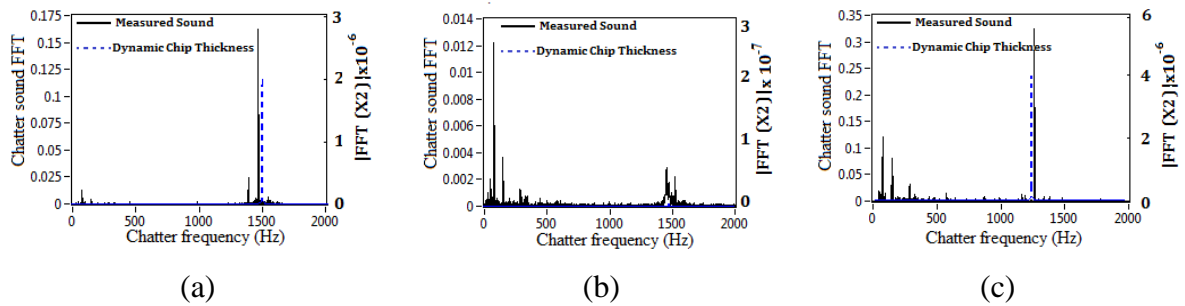

Figure 4.7. Frequency spectrums of the measured sound and the dynamic chip thickness of the second cutter simulated in time domain for points (a) A, (b) B and (c) C.

Through these results, it is proven that the parallel operation provides higher stability limits. Even though the stable depths for the first and the second tools are 0.82 and 1 mm when they are used in single tool turning, using the parallel operation the stable depth of cut can exceed 3 and 4 mm for the first and second tools, respectively, representing at least 600% increase in total stable MRR in comparison with single mode turning. Also, the line $b_2 = b_1$ intersects the stable boundary at $b_2 = b_1 = 3.1$ mm, demonstrating stable limit for the case where tools remove identical depth of cut. Although the parallel turning with identical depth of cuts has relatively high MRR in comparison with single tool turning, the highest productivity occurs at the right top corner of the stability map. At this point, flexibility ratio of the tools is the decisive factor in determining the maximum productivity. It has been indicated through the simulations, for cases which tools have similar dominant vibrating modes, their dynamic transfer function will be amplified at chatter frequencies and the stability decreases drastically. However, when natural frequencies of the tools are close to each other (not identical), the dynamic transfer functions will decrease and in turn lead to enhanced stability boundaries (see Figure 4.8)
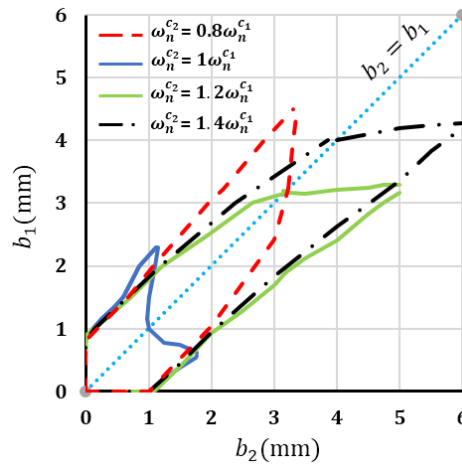
31

Figure 4.8. Stability map variation for different natural frequency ratio of the tools, ($r_1 = r_2$=0.4 mm, $\omega_n^{c_1}$=1178.6 Hz) at 1500RPM

Effect of insert's nose radius and side edge angle on the stability map is demonstrated in Figure 4.9. In the current case, using inserts having higher nose radii and side edge angles resulted in slightly enlarged stability maps due to the reduced contribution of the tools' dynamics in the feed direction.

(a)

(b)
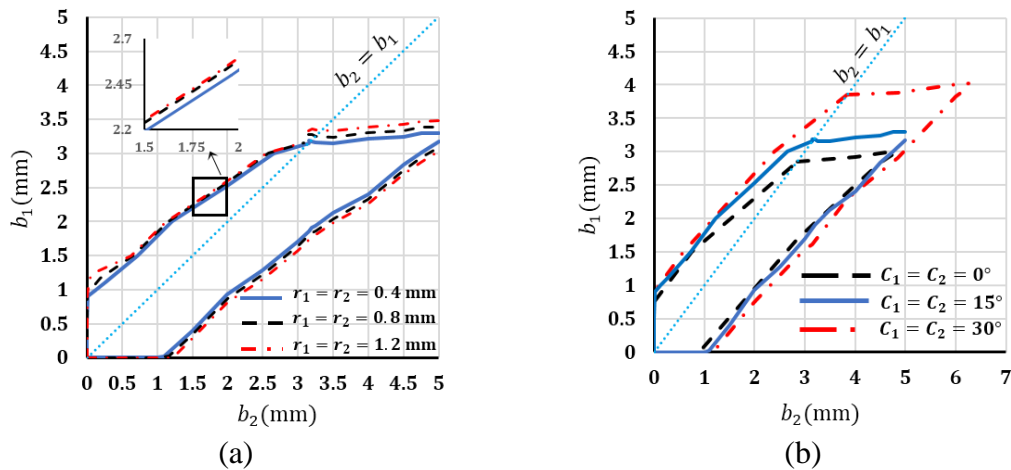
Figure 4.9. Variation of stability map with different nose radius values ($C_1 = C_2 = 15°$) (a) and side edge cutting angles ($r_1 = r_2 = 0.4\ mm$) (b) at 1500 RPM.

4.2. Cutting Different Surfaces

4.2.1. Flexible Workpiece

In this case, in contrast with previous two cases, tools do not cut the same surface. In fact, the essence of this configuration is to execute a parallel turning operation where one of the cutters performs roughing while the other one finishes the generated surface left by the first cutter. The workpiece material is AISI 1050 with length and diameter of 113mm

and 47mm, respectively (Figure 4.10). Similar with case 1, workpiece is more flexible than the cutters. Dynamic properties of the workpiece are presented in Table 5.
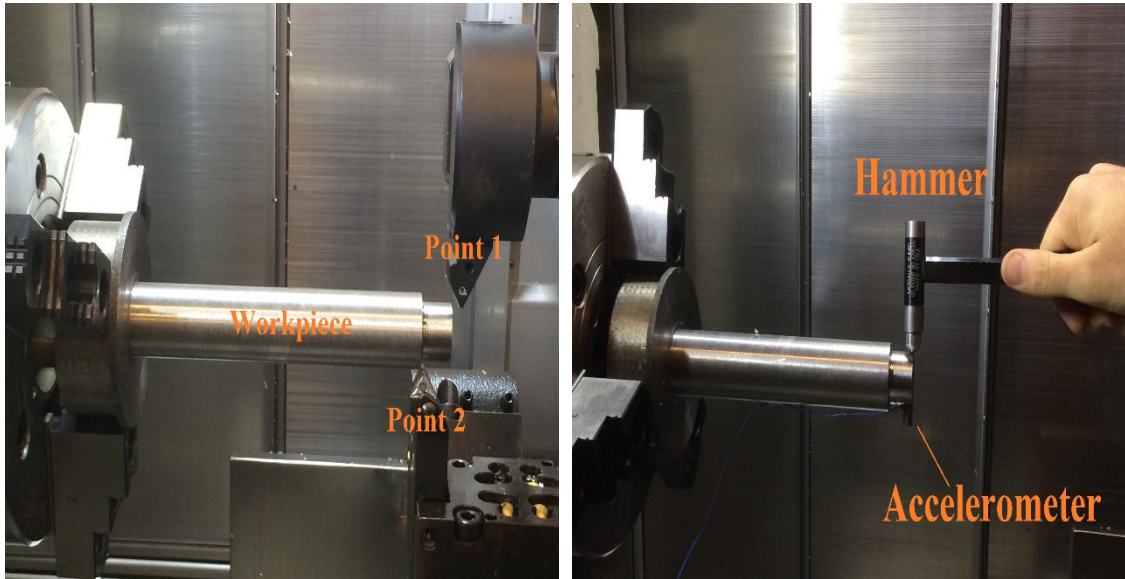
Figure 4.10. Modal data measurements and tool/workpiece configuration

Table 5, Modal data of the workpiece [case 3]

Workpiece	f_n(Hz)	Stiffness(N/m)	Damping (%)
$G_{yy}^{w1,1}$	586	1.388×10^7	1.125
$G_{yy}^{w2,1} \cong G_{yy}^{w1,2}$	587	1.609×10^7	1.303
$G_{yy}^{w2,2}$	585	1.5434×10^7	1.713

Tool geometries, the force coefficients and modal data of the lower and upper tools are identical with those of case 1 (See Table 1 and Table 2).

33

Figure 4.11. (a) Stability map predicted by frequency solution and time domain model at 1500 RPM (b) Dynamic chip thickness for three different points at b2=1.75mm. (c) Chatter marks left on the surface in stable and unstable processes.

Results of frequency and time domain simulations are illustrated in Figure 4.11.a. In this case, the stability limit for single tool operations at point 1 and 2 are calculated as 0.49 and 1.25 mm, respectively [28]. Obviously, point 1 is more flexible in the radial direction in com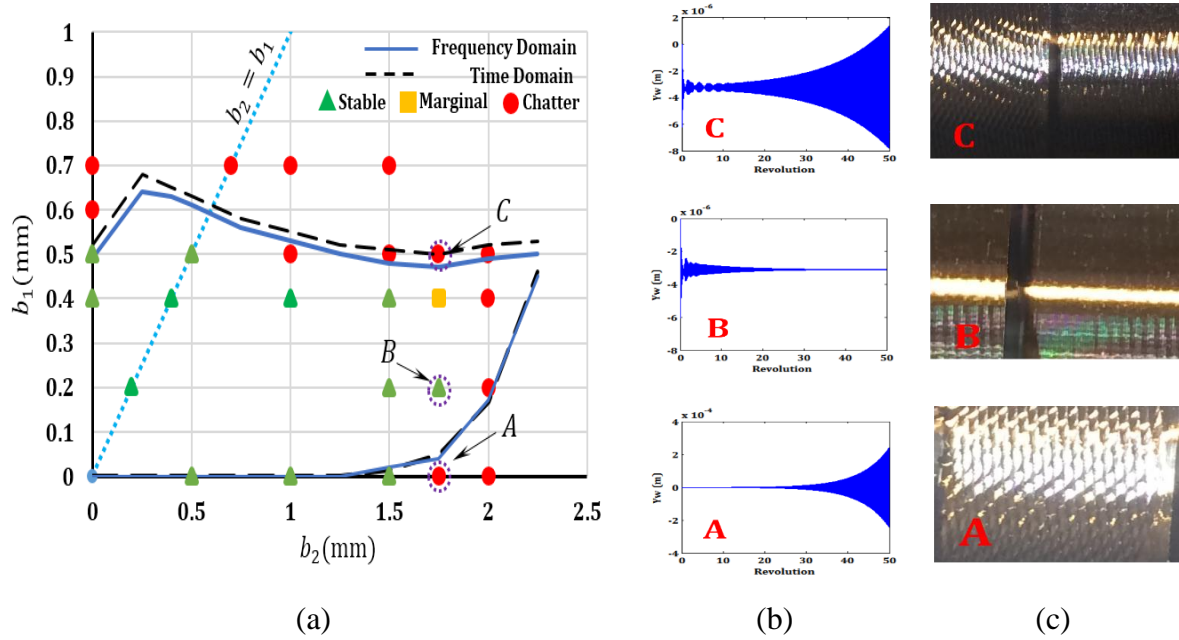parison with point 2 since it is located farther from the clamping point. For $b_1 >$ 0.49 mm , the parallel operation becomes unstable regardless the amount of increase in b_2 since the generated radial force increases considerably and it cannot be sufficiently countered by the radial force generated by the second cutter. However, for $b_2 > 1.25$ mm values, process may remain within stable upper and lower limits by proper selection of b_1 indicating that radial force acting upon the first tool can cancel the second tool's radial force. To be representative, dynamic displacements of the workpiece for b_2=1.75mm and three b_1 values (0, 0.2 and 0.5 mm) are simulated in the time domain model and illustrated in Figure 4.11.b. Additionally, the generated surface after the cut for three experimental points, i.e. A, B and C, are shown in Figure 4.11.c.
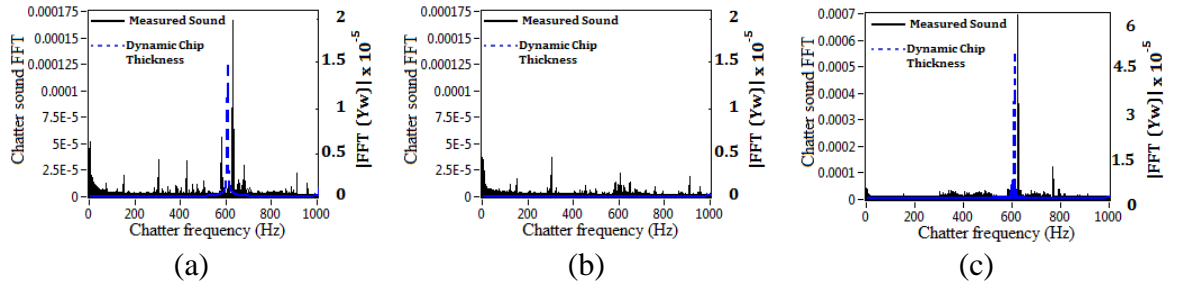
Figure 4.12. Frequency spectrums of the measured sound and dynamic displacements of the workpiece simulated in the time domain for points (a) A, (b) B and (c) C.

Furthermore, FFT of the chatter sound and workpiece dynamic displacement in time domain simulations at experiment points A, B and C demonstrate a good agreement with the predictions (see Figure 4.12). Proper parameter selection can ensure enhanced chatter-free productivity. The line $b_1 = b_2 = 0.56$ mm is the maximum achievable productivity when both tools have identical depth of cuts. However, by selecting point $b_1 = 2$ mm and $b_2 = 0.45$ mm, not only a stable cut is guaranteed, but also MRR of the process increased more than 100 percent.
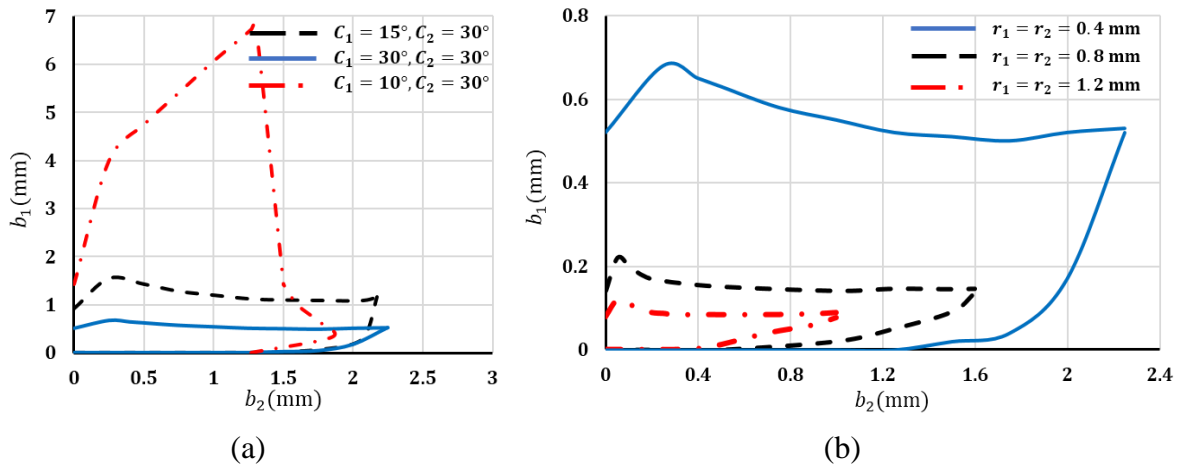
Figure 4.14. Variation of stability map with different nose radius values ($C_1 = C_2 = 30°$) (a) and side edge cutting angles ($r_1 = r_2 = 0.4\ mm$) (b) at 1500 RPM.

An advantage of using parallel turning for cutting different surfaces compared with parallel turning for cutting a shared surface is the possibility of utilizing tools with different side edge angles. Proper selection of the side edge angle may result in enlarged stability maps. As can be seen in Figure 4.14.a, where $C_1 = 30°, C_2 = 30°$, the cross-transfer functions between the two contact points are not strong enough to counter the radial force acting upon the first tool, and thus, by increasing b_1 beyond first tool's stable limit in single turning mode, system will be unstable regardless of b_2 values. However, by decreasing C_1 to 10°, the radial force acting on the first tool decreases, and therefore

35

cross transfer functions between the contact points are strong enough to decrease the total radial force acting on the first point. Consequently, for b_1 values bigger than first tool's stable limit in single turning mode, system enters a new stability zone and can be stable by proper setting of the b_2. The maximum MRR in the latter example, i.e. $C_1 = 10°, C_2 = 30°$, is 210% higher than the maximum MRR in the former one, i.e. $C_1 = 30°, C_2 = 30°$. Additionally, increasing insert's nose radius results in higher contribution of workpiece dynamics; and hence, shrunk stability maps (see Figure 4.14.b).

4.2.2. Flexible Tools

In this case, two flexible cutting tools were clamped on a turret where the workpiece is considered as rigid (see Figure 4.15). To verify the proposed model, the experimental results presented in [31] are compared with the simulation results obtained in this work. The cutting force coefficients of the tools were identified as 872 MPa in the feed direction [31]. In the tests in [31], the second tool was clamped in a way that its depth of cut (b_2) is 4.7mm, and based on given b_2, stable depth of cut of the first tool in parallel operation was calculated. The dynamic properties of the tools are presented in Table 6 [31].
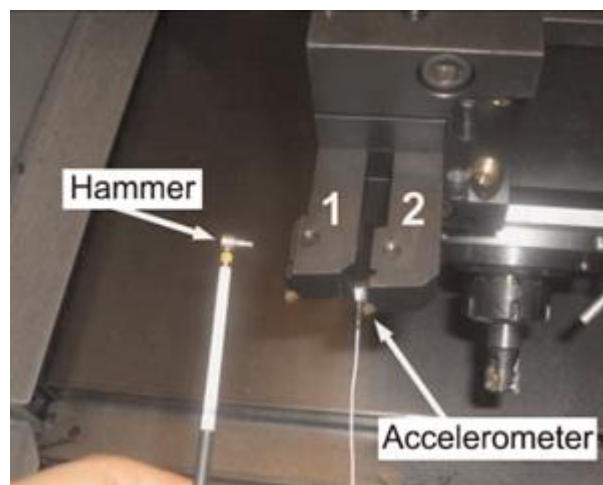

Figure 4.15. Flexible tool mounted on a turret [31].

Table 6, Dynamic properties of the tools [31]

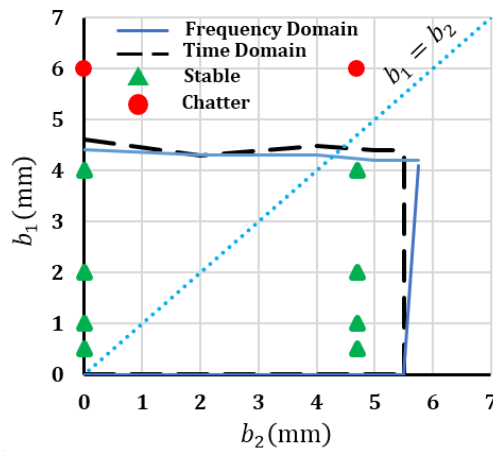|	Mode	f_n(Hz)	Damping (%)	k(N/m)
G_{11}	1	2086.1	5.71	4.875×10^7
	2	2290.7	1.61	2.272×10^8
	3	3899.9	1.22	3.591×10^8
$G_{12} = G_{21}$	1	2067.1	5.55	1.635×10^8
	2	3572.7	5.35	-2.189×10^8
G_{22}	1	2050.7	4.78	6.753×10^8
	2	2553.9	2.87	8.602×10^8
	3	3036.1	6.09	5.903×10^7
	4	3443.5	1.29	3.141×10^8
	5	3629.6	1.61	3.069×10^8

Figure 4.16. Absolute stability limit for b_1 in frequency solution and time domain model at 745 RPM for given b_2. Side edge cutting angle is 0° and nose radii is 0.4 mm. Experiments are adopted from [31].

Stable depth of cuts for the first and the second tools in a single tool operation were determined as 4.4 and 5.5 mm, respectively, considering true geometry of the inserts based on the provided model in [28]. However, in the parallel configuration, the stability limit for the first tool was calculated as 4.3 mm for given $b_2 = 4.7mm$. As it can be seen from the stability map presented in Figure 4.16, unlike previous parallel turning operations, when depth of cut of the second cutter increases beyond its stability limit in the single tool turning mode, the process becomes unstable. This means that there are no multiple stable and unstable zones which is due to the fact that the cross-transfer functions between the tools are not strong enough to attenuate the dynamic forces. Even though the limit for the first tool slightly decreased in parallel operation in comparison with the single tool case, the MRR in parallel operation increased 100 % approximately. However, as can be seen in Figure 4.16, maximum MRR occurs at point $b_2 = 5.5$ and $b_1 = 4.3$ mm

at the top right corner of the stability map. In accord with this fact, appropriate parameter selection in parallel turning operations will result in improved productivity.

Effects of nose radii and side edge cutting angle on the stability map is illustrated by Figure 4.17. Similar with previous case, possibility of using tools with different side edge cutting angles can be employed for enhanced productivity. Increasing the side edge cutting angle and nose radius of the inserts slightly expand the stable boundaries (see Figure 4.17). It should be noted that effect of nose radii and side edge cutting angle on the stability maps is more significant when the workpiece is flexible. In fact, in parallel turning of a flexible workpiece, increasing nose radii and side edge angle add flexibility to the system which results in extremely contracted stability maps. However, in parallel turning with flexible tools, increasing inserts' nose radii and side edge angle add rigidity to the system which in turn lead to slightly enlarged maps.
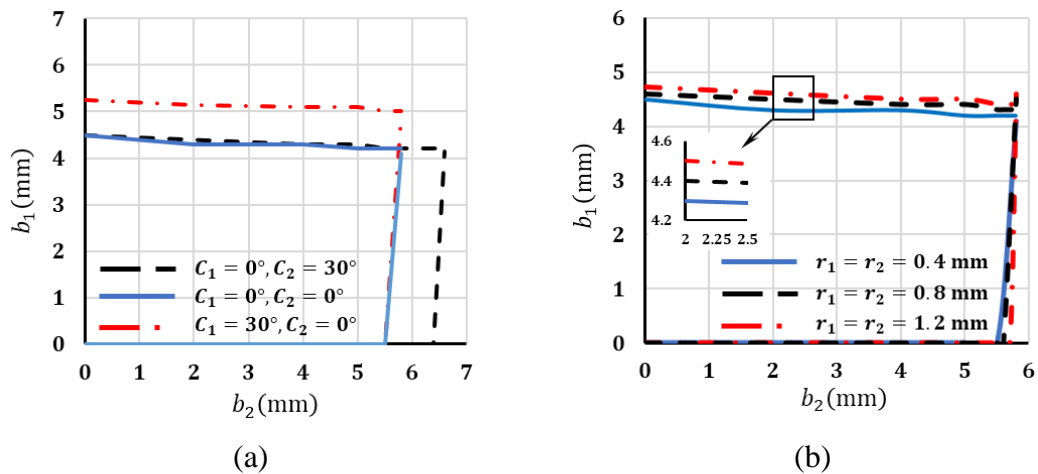
Figure 4.17. Variation of stability map with different nose radius values ($C_1 = C_2 = 0°$) (a) and side edge cutting angles ($r_1 = r_2 = 0.4 \, mm$) (b) at 745 RPM.

4.3. Effect of Relative Flexibility of Components on the Stability Maps

Practically speaking, in majority of parallel turning operations, one of the system's directions is much more flexible than the other directions. Hence, the vibration either in the feed direction or the radial direction contribute to the regenerative chatter individually. However, in order to show the ability of the formulation to capture the bi-directional chatter behavior in the parallel turning, the structure assumed to be flexible in two (feed and radial) directions simultaneously. In this section, three different workpieces to tools stiffness ratio has been considered and in each case, effect of the nose radii on the stability

map of first configuration of parallel turning has been investigated. There is a significant dependency of stability map on the effect of nose radius. The dynamics of the system components are listed in Table 7 and Table 8 as bellow:

Table 7. Natural frequency and damping of the system's component

Component	Mode	f_n(Hz)	Damping (%)
Workpiece	1	586	1.7
Upper Tool	1	1178.6	1.5
Lower Tool	1	1452.3	1.1

Table 8. stiffness ratios of the tools and the workpiece

Component	$K_w/K_c =10$	$K_w/K_c =1$	$K_w/K_c =0.1$
Workpiece	80×10^6	8×10^6	8×10^6
Upper Tool	8×10^6	8×10^6	80×10^6
Lower Tool	8×10^6	8×10^6	80×10^6

Force coefficients have been calibrated as 692 and 178 N/mm^2 for the feed and the radial directions respectively. Tools have 0° of side edge cutting angle, 5° of inclination angle.
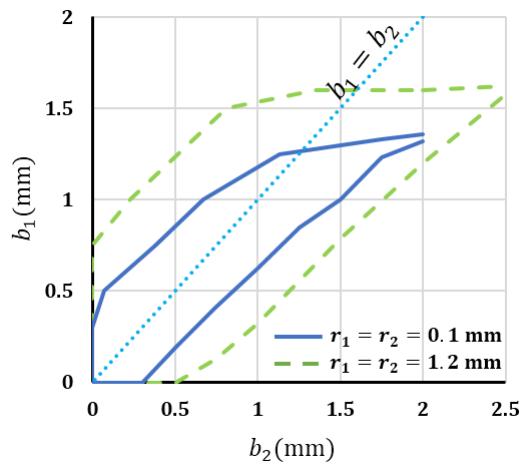

Figure 4.18. Stability map variation for $K_w/K_c =10$

Generally, increasing the nose radius and/or side edge cutting angle lead to higher resultant forces in the radial directions and smaller forces in the feed direction. Accordingly, depending on the flexibility of each direction of the system, effect of the

nose radii variation will be different. In case of flexible tools (see Figure 4.18), by using inserts having higher nose radius, smaller forces act upon the flexible direction, i.e. feed direction. Hence, the stability map enlarges. However, amount of enlargement in the stability map due to the increasing the nose radii depends on the flexibility of the tools. In fact, the more flexible tools, the more enlargement in the stability map. In case of flexible workpiece, the effect of the nose radii variation on the stability maps is more critical. Resultant forces for an insert having 0.1 mm nose radius, are mostly in the feed direction. Therefore, stability map will not be substantially influenced by the flexibility in the radial direction (see Figure 4.19.a). In fact, the contribution of cutters' dynamics outweighs those of the workpiece. However, by increasing the nose radii to 1.2 mm, contribution of workpiece's dynamics drastically increases and will lead to an extremely small stability map (see Figure 4.19.b).

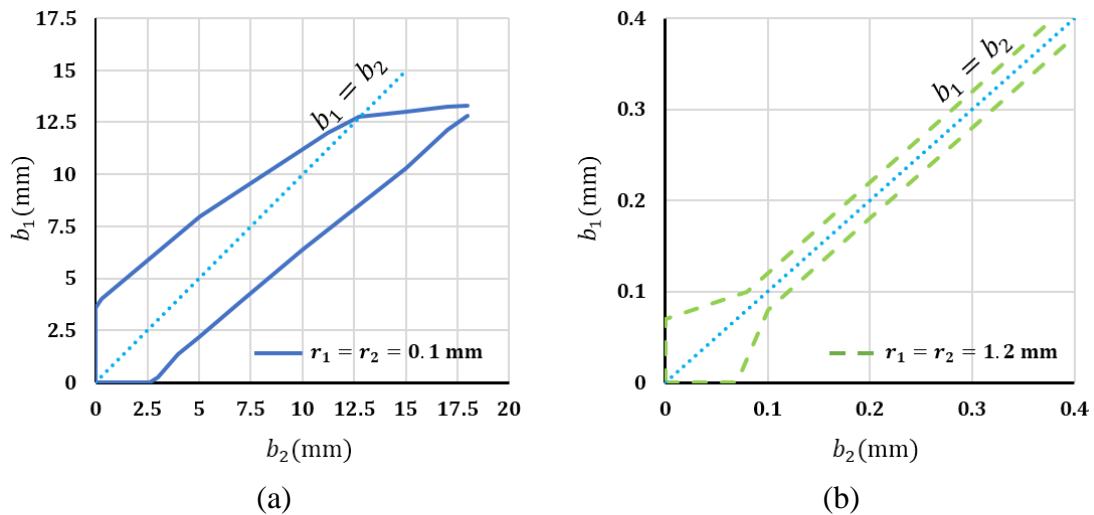(a)   (b)

Figure 4.19. Stability map variation for $K_w/K_c = 0.1$

When the flexibility of the directions is comparable (see Figure 4.20), even though the workpiece is as flexible as the cutters, inserts having 0.1 cannot provide enough forces in the radial direction; hence, cutters are the dominant flexible component. Nonetheless, by increasing the nose radii to 0.4 mm, considerable amount of forces will be projected in the radial direction which in turn results in higher contribution of the workpiece dynamics; shrinking the stability map noticeably. Figure 4.21 demonstrates occurrence of chatter for two close points at different chatter frequencies (Figure 4.20.b), implying different component contributing in chatter instability. Point A is below the lower level of the stability map, and is chattering because resultant forces in the radial direction is high, therefore, workpiece dynamics contribute to the chatter instability (see Figure

4.21.a). In contrary, point B, lies on the line $b_1 = b_2$ in which radial forces are cancelling each other, suppressing the workpiece's vibration. Chatter instability of point B is due to the upper cutter's dynamics, as it clearly illustrated by Figure 4.21.b.
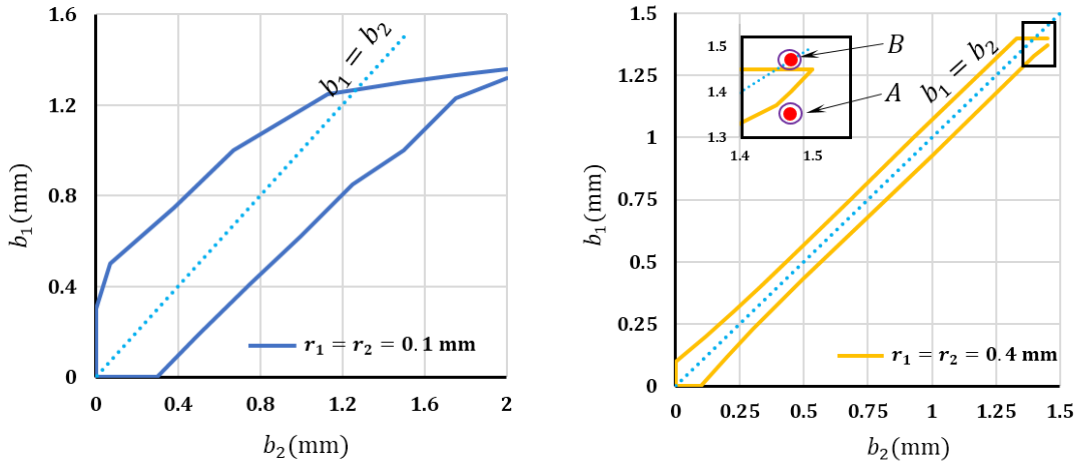

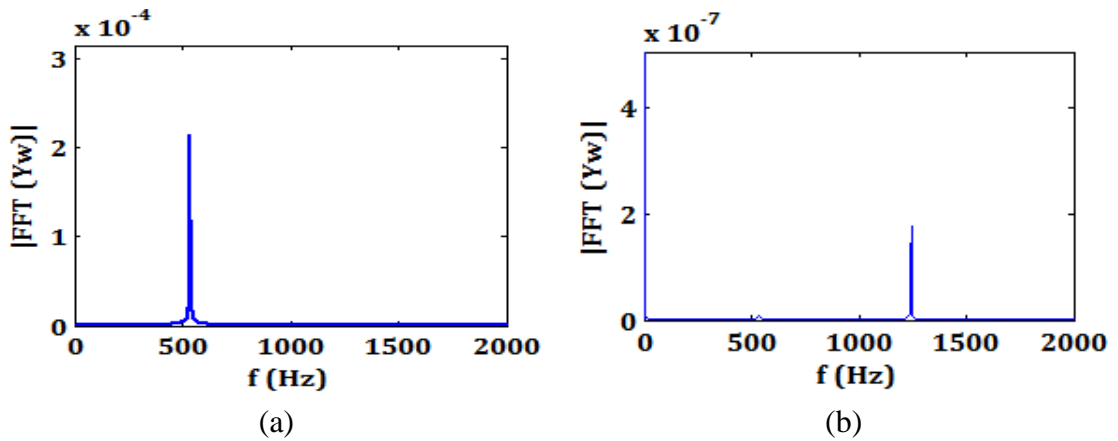Figure 4.20. Stability map variation for $K_w/K_c = 1$

(a)   (b)

Figure 4.21. Chatter occurrence at different frequencies for point A and B

Chapter 5 SUMMARY AND CONCLUSION

In this thesis, a multi-dimensional chatter stability model for parallel turning operation is presented and solved for various cutting strategies considering the tools and workpiece dynamic compliance effect in frequency and time domain. The model predictions were verified by the experiments. Parallel turning potential to enhanced cutting performance can be achieved by selecting the proper parameters for the process and cutter geometry based on the developed stability maps. By setting depth of cut for each cutter in parallel mode below the critical depths of cutters in corresponding single tool modes, MRR increases due to existence of two tools simultaneously removing material. However, the maximum performance, i.e. MRR, will be obtained in the top corner of the stability maps. In accordance with the results, insert nose radii and side edge cutting angle has different effects on the stability map variation. Increasing insert's nose radius and side edge cutting angle severely shrink the stability map of parallel turning of flexible workpiece. In contrast, increasing the nose radii and side edge angle slightly enlarge the stability map of parallel turning with flexible tools. Following practical measures can be recommended to enhance productivity:

- In parallel turning of flexible workpieces, the maximum stability limit is achieved when identical cutters (having same depth of cut and insert geometry) machine a shared surface. It is due to the fact that identical radial forces cancel dynamic forces in the radial direction.
- In parallel turning of different surfaces of flexible workpieces, the maximum stability is achieved when the total radial dynamic forces acting on the workpiece is minimized; hence using identical cutters with same depth of cuts will not necessarily lead to maximum MRR because of different dynamics properties of the contact points. Nonetheless, using a tool which generates

smaller radial forces on that contact point of the workpiece which has smaller stiffness is a measure to enlarge the stability maps. Inserts with smaller force coefficients, nose radius and side edge angle exert smaller radial forces.

- Adjusting the axial offset between the cutters and being restricted to utilize inserts with similar side edge cutting angles are disadvantages of employing parallel turning operation on a shared surface.
- In parallel turning with flexible tools which cut a shared surface, maximum stability limit occurs while utilizing tuned tools where absorbing effect of tools is maximum [31].

Chapter 6 **BIBLIOGRAPHY**

[1] F. W. Taylor, *On the art of cutting metals*. New York, The American Society of Mechanical Engineers,[1907], 1907.

[2] J. Tlusty and M. Polacek, "The stability of machine tools against self-excited vibrations in machining," *Int. Res. Prod. Eng.*, vol. 1, no. 1, pp. 465–474, 1963.

[3] S. A. Tobias and W. Fishwick, "The chatter of lathe tools under orthogonal cutting conditions," *Trans. ASME*, vol. 80, no. 2, pp. 1079–1088, 1958.

[4] J. Tlusty, *Manufacturing processes and equipment*. Prentice Hall, 2000.

[5] J. Munoa *et al.*, "Chatter suppression techniques in metal cutting," *CIRP Ann. Technol.*, vol. 65, no. 2, pp. 785–808, 2016.

[6] H. E. Merritt, "Theory of self-excited machine tool chatter," *J. Eng. Ind.*, vol. 87, no. 4, pp. 447–454, 1965.

[7] F. Koenigsberger and J. Tlusty, *Machine tool structures*. Elsevier, 2016.

[8]   J. Tlusty and F. Ismail, "Basic non-linearity in machining chatter," *CIRP Ann. Technol.*, vol. 30, no. 1, pp. 299–304, 1981.

[9]   J. Tlusty, "Dynamics of high-speed milling," *J. Eng. Ind.*, vol. 108, no. 2, pp. 59–67, 1986.

[10]   S. Smith and J. Tlusty, "Efficient simulation programs for chatter in milling," *CIRP Ann. Technol.*, vol. 42, no. 1, pp. 463–466, 1993.

[11]   I. Minis, R. Yanushevsky, A. Tembo, and R. Hocken, "Analysis of linear and nonlinear chatter in milling," *CIRP Ann. Technol.*, vol. 39, no. 1, pp. 459–462, 1990.

[12]   B. Yanushevsky, "A new theoretical approach for the prediction of machine tool chatter in milling," *J. Eng. Ind.*, vol. 115, p. 1, 1993.

[13]   Y. Altinta\cs and E. Budak, "Analytical prediction of stability lobes in milling," *CIRP Ann. Technol.*, vol. 44, no. 1, pp. 357–362, 1995.

[14]   Y. Altintas and E. Budak, "Analytical prediction of chatter stability in milling—part II: application of the general formulation to common milling systems," *J. Dyn. Syst. Meas. Control*, vol. 120, no. 1, pp. 31–36, 1998.

[15]   Y. Altintas and E. Budak, "Analytical prediction of chatter stability in milling—part I: general formulation," *J. Dyn. Syst. Meas. Control*, vol. 120, pp. 22–30, 1998.

[16]   T. Insperger and G. Stépán, "Semi-discretization for time-delay systems: stability and engineering applications." Springer Science & Business Media, 2011.

[17]   A. Comak and E. Budak, "Modeling dynamics and stability of variable pitch and helix milling tools for development of a design method to maximize chatter stability," *Precis. Eng.*, vol. 47, pp. 459–468, 2017.

[18]   S. Engin and E. Budak, "Analytical stability prediction and design of variable pitch cutters," *J. Manuf. Sci. Eng.*, vol. 121, p. 173, 1999.

[19]   Y. Altintas, M. Eynian, and H. Onozuka, "Identification of dynamic cutting force coefficients and chatter stability with process damping," *CIRP Ann. Technol.*, vol. 57, no. 1, pp. 371–374, 2008.

[20]   E. Budak and L. T. Tunc, "Identification and modeling of process damping in

turning and milling using a new approach," *CIRP Ann. Technol.*, vol. 59, no. 1, pp. 403–408, 2010.

[21]   Y. Yang, J. Munoa, and Y. Altintas, "Optimization of multiple tuned mass dampers to suppress machine tool chatter," *Int. J. Mach. Tools Manuf.*, vol. 50, no. 9, pp. 834–842, 2010.

[22]   U. Yigit, E. Cigeroglu, and E. Budak, "Chatter reduction in boring process by using piezoelectric shunt damping with experimental verification," *Mech. Syst. Signal Process.*, vol. 94, pp. 312–321, 2017.

[23]   X. Lu, F. Chen, and Y. Altintas, "Magnetic actuator for active damping of boring bars," *CIRP Ann. Technol.*, vol. 63, no. 1, pp. 369–372, 2014.

[24]   M. Azvar and E. Budak, "Multi-dimensional modelling of chatter stability in parallel turning operation," 2016.

[25]   E. Budak and E. Ozturk, "Dynamics and stability of parallel turning operations," *CIRP Ann. Technol.*, vol. 60, no. 1, pp. 383–386, 2011.

[26]   C. Brecher, A. Epple, S. Neus, and M. Fey, "Optimal process parameters for parallel turning operations on shared cutting surfaces," *Int. J. Mach. Tools Manuf.*, vol. 95, pp. 13–19, 2015.

[27]   B. C. Rao and Y. C. Shin, "A comprehensive dynamic cutting force model for chatter prediction in turning," *Int. J. Mach. Tools Manuf.*, vol. 39, no. 10, pp. 1631–1654, 1999.

[28]   E. Budak and E. Ozlu, "Analytical modeling of chatter stability in turning and boring operations: a multi-dimensional approach," *CIRP Ann. Technol.*, vol. 56, no. 1, pp. 401–404, 2007.

[29]   I. Lazoglu, M. Vogler, S. G. Kapoor, and R. E. DeVor, "Dynamics of the simultaneous turning process," *Trans. Am. Manuf. Res. Inst. SME*, pp. 135–140, 1998.

[30]   O. B. Ozdoganlar and W. J. Endres, "Parallel-process (simultaneous) machining and its stability," in *IMECE/ASME International Mechanical Engineering Congress and Exposition, Nashville, Tennessee, Nov*, 1999, pp. 14–19.

[31]   E. Ozturk, A. Comak, and E. Budak, "Tuning of tool dynamics for increased stability of parallel (simultaneous) turning processes," *J. Sound Vib.*, vol. 360, pp.

17–30, 2016.

[32]   M. J. Reith, D. Bachrathy, and G. Stepan, "Optimal Detuning of a Parallel Turning System—Theory and Experiments," *J. Dyn. Syst. Meas. Control*, vol. 139, no. 1, p. 14503, 2017.

[33]   M. J. Reith, D. Bachrathy, and G. Stepan, "Improving the stability of multi-cutter turning with detuned dynamics," *Mach. Sci. Technol.*, vol. 20, no. 3, pp. 440–459, 2016.

[34]   M. J. Reith and G. Stepan, "Effect of non-proportional damping on the dynamics and stability of multi-cutter turning systems," *Int. J. Mach. Tools Manuf.*, vol. 117, pp. 23–30, 2017.

[35]   R. Sipahi and N. Olgac, "A unique methodology for the stability robustness of multiple time delay systems," *Syst. Control Lett.*, vol. 55, no. 10, pp. 819–825, 2006.

[36]   Y. Altintas, *Manufacturing automation: metal cutting mechanics, machine tool vibrations, and CNC design*. Cambridge university press, 2012.

[37]   D. Bachrathy, "Multi-dimensional bisection method (mdbm)." 2012.

[38]   D. Bachrathy and G. Stépán, "Bisection method in higher dimensions and the efficiency number," *Period. Polytech. Eng. Mech. Eng.*, vol. 56, no. 2, p. 81, 2012.

[39]   M. U. Guide, "The mathworks," *Inc., Natick, MA*, vol. 5, p. 333, 1998.

[40]   C. F. Gerald, *Applied numerical analysis*. Pearson Education India, 2004.

[41]   Y. Altinta and E. J. A. Armarego, "Prediction of milling force coefficients from orthogonal cutting data," *Trans. ASME J. Engng Ind*, 1996.